Dynamic Characteristics of a Cantilever Beam with Transverse Cracks

R. K. Behera and D. R. K. Parhi

Department of Mechanical Engineering, National Institute of Technology, Rourkela, 769008, Orissa, India

S. K. Sahu

Department of Civil Engineering, National Institute of Technology, Rourkela, 769008, Orissa, India

It has long been observed that the dynamic response of a structure changes due to the presence of a crack. Scientific analysis of such phenomena can be utilised for fault diagnosis and the detection of cracks in structures. The present investigation is an attempt in that direction. Theoretical expressions have been developed in order to determine the natural frequencies and mode shapes for an elastic cantilever beam with two cracks using flexibility influence coefficients and a local stiffness matrix. The numerical results for the beams without cracks, with one crack, and with two cracks are compared. It has been observed from the numerical results that there are appreciable changes in the vibration characteristics of the cantilever beam with and without cracks. This method can be utilised for multi crack identification of structures.

Nomenclature

a_1	− depth of crack
a_2	− depth of crack
A	− cross-sectional area of beam
$A_i, i = 1, 18$	− unknown coefficients of matrix A
B	− width of the beam
W	− depth of beam
B_1	− vector of exciting motion
$c_u = (E/\rho)^{1/2}$	
$c_y = (EI/\mu)^{1/2}$	
E	− Young's modulus of elasticity
$F_i, i = 1, 2$	− experimentally determined function
i, j	− variables
J	− strain-energy release rate
$K_{Ii}, i = 1, 2$	− stress intensity factors for P_i loads
$\bar{k}_u = \omega L / c_u$	
$\bar{k}_y = (\omega L^2 / c_y)^{1/2}$	
K_{ij}	− local flexibility matrix element
L	− length of beam
L_1, L_2	− location of the crack from fixed end
$M_i, i = 1, 4$	− compliance constant
$M_{ij} = M_i / M_j$	
$P_i, i = 1, 2$	− axial force ($i = 1$), bending moment ($i = 2$)
K	− stiffness matrix for free vibration
K', K''	− stiffness matrix of first and second crack locations
$u_i, i = 1, 3$	− normal functions (longitudinal) $u_i(x)$
x	− co-ordinate of the beam
y	− co-ordinate of the beam
Y_0	− amplitude of the exciting vibration
$y_i, i = 1, 3$	− normal functions (transverse) $y_i(x)$
ω	− natural circular frequency
β_1	− relative crack location (L_1/L)
β_2	− relative crack location (L_2/L)
$\mu = A\rho$	
ρ	− mass density of the beam
v	− Poison's ratio
ξ_1	− relative crack depth (a_1/W)
ξ_2	− relative crack depth (a_2/W)
$|Q|$	− determinant of Q

1. INTRODUCTION

For the last several years, a considerable amount of research work has been undertaken to investigate the faults in structures. It has been observed that most of the structural members fail due to the presence of cracks. The cracks are developed mainly due to fatigue loading. Therefore the detection of cracks is an important aspect of structural design. A crack that occurs in a structural element causes some local variation in its stiffness, which affects the dynamic behaviour of the element and the whole structure to a considerable degree. The frequencies of natural vibration, amplitudes of forced vibration, and areas of dynamic stability change due to the existence of such cracks.[1-5] An analysis of these changes makes it possible to identify the magnitude and location of the crack. This information enables one to determine the degree of sustainability of the structural element and the whole structure.

Regarding the above problem, Cawley et al.[6] have combined sensitivity analysis with FEM to determine crack location. The coupling of vibration modes of vibration of a clamped – free circular cross-section Timoshenko beam with a transverse crack was investigated by Papadopoulos and Dimarogonas.[7] The crack is simulated using a 6×6 local flexibility matrix. The nondiagonal terms of this matrix cause coupling between the longitudinal, torsional, and bending vibrations. The researchers observed that the method used is very sensitive even in the case of small cracks.

Gudmundson[8] has investigated the transverse vibration of a cracked beam experimentally to validate a perturbation method which he had developed. He observed that depending upon the crack location, a crack may remain completely open, partially open, or closed if the vibration amplitudes are

too small. Chondros and Dimarogonas[9] have considered the crack as a local elasticity which affects the whole cracked structure under consideration, and they related the crack depth with the decrease in frequency.

Gounaris and Papazoglou[10] have used a mixed finite-boundary element method to study the dynamic behaviour of a cracked Timoshenko beam. They have vibrated the beam in air and in water in plain bending, using two degrees of freedom for each mode. Papadopoulos et al.[11] have used a 6×6 compliance matrix to simulate a cracked shaft and to study its dynamic behaviour. They concluded that the presence of a crack affects the modes of vibration.

Papadopoulos and Dimarogonas[12] have described the coupling of the bending and longitudinal vibration of a stationary cracked shaft with an open crack. The crack is modelled using a 2×2 local flexibility matrix with coupling terms. The elements of this matrix are obtained analytically. The free vibration of the shaft and the influence of this crack on the vibrational behaviour of the shaft are analysed.

Dimarogonas and Massours[13] have investigated the dynamic behaviour of a circumferentially cracked shaft in torsion and proposed nomographs for finding the crack depth and location.

A diagnostic method of determining the position and size of a transverse open crack on a stationary shaft without disengaging it from the machine system was investigated by Tsai and Wang.[14] The crack is modelled as a joint of a local spring. To obtain the dynamic characteristics of a stepped shaft and a multi-disc shaft, the transfer matrix method is employed on the basis of the Timoshenko beam theory. The post-buckling behaviour of a cracked column with an edge crack was studied by Anifantis and Dimarogonas.[15]

The prediction and identification of transverse cracks in beams with different end conditions were studied by Mohammad.[16] He has developed an algorithm for crack identification. The input data for his algorithm are the natural frequencies of the first two bending modes of vibration of the damaged beam. Using these two input values, and with the availability of accurate frequency measurements and ideal end conditions, the crack location and depth are identified in terms of known beam parameters.

A numerical method was described by Chinchalkar[17] for determining the location of a crack in a beam of varying depth when the lowest three natural frequencies of the cracked beam are known. The crack is modelled as a rotational spring. The graphs of the spring stiffness versus crack location are plotted for each natural frequency to find out the crack location.

A theoretical and experimental study of the dynamic behaviour of different multi-beams systems with a transverse crack was presented by Saavedra and Cuitino.[18] The additional flexibility that the crack generates in its vicinity is evaluated using the strain energy density function. Based on this flexibility, a new cracked finite element stiffness matrix is deduced. The proposed element is used to evaluate the dynamic response of a cracked free-free beam subjected to a harmonic force.

The experimental vibration behaviour of a free-free beam with a breathing crack was simulated by Jyoti et al.[19] The cracked beam is simulated for a sinusoidal input force using a simple finite element model. The simulation results are compared with an earlier study and found to be more realistic.

The fundamental frequency of cracked Euler-Bernoulli beams in bending vibrations was studied analytically by Fernandez and Navaro.[20] They have solved the problem using the flexibility influence function which leads to an eigenvalue problem formulated in integral form.

In the present paper, an analytical-computational technique has been developed for vibration analysis of the cantilever beam with cracks. The numerical results are compared with the experimental results in order to confirm the authencity of the theory developed.

2. LOCAL FLEXIBILITY OF A CRACKED BEAM UNDER BENDING AND AXIAL LOADING

Transverse surface cracks of depths a_1 and a_2 are considered on a beam of length L. The beam has local flexibilities which are affected in many directions by the cracks. The resulting flexibilities depend on the direction of the applied forces. The beam has a depth W and a width B. The beam is assumed to be loaded with an axial tensile force P_1 and a bending moment P_2 (shown in Fig. 1). The bending moment has a direction so that its influence opens the crack. The axial force P_1 and bending moment P_2 provide coupling with the longitudinal and transverse vibration motion. For these loadings, the additional displacement u_i along the direction of forces P_i due to the presence of the cracks are computed using Castigliano's theorem[21] and by generalisation of the Paris equation, under the assumption of linear, elastic fracture mechanics conditions.
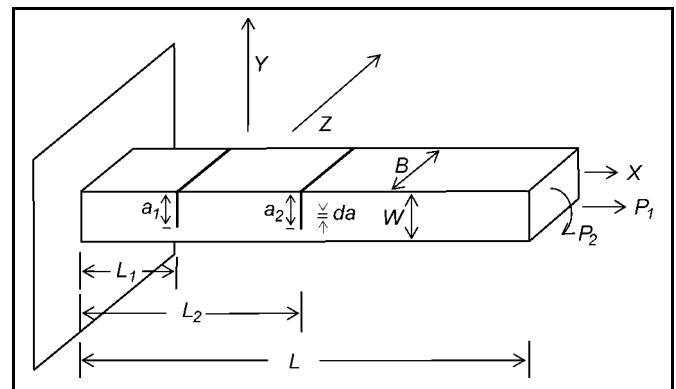

Figure 1. Geometry of cantilever beam.

In general, the strain energy of a fracture section can be written as:

$$U_T = \int_{A_f} \frac{\partial U_T}{\partial A_f} dA_f,$$ (1)

where U_T is the total strain energy due to the crack and A_f is the surface of the fractured section. The energy release rate J is given by:

$$J = \frac{\partial U_T}{\partial A_f}.$$ (2)

Using Eqs. (1) and (2), one can find

$$U_T = \int_{A_f} J dA_f .$$ (3)

From Castigliano's theorem,[21] the displacements u_i are

$$U_T = \frac{\partial U_T}{\partial P_i}, \qquad (4)$$

where u_i are the relative displacements in the neighbourhood of the crack and P_i are the corresponding loads. The compliance factors are determined by

$$C_{ij} = \frac{\partial u_i}{\partial P_j}, \qquad (5)$$

where C_{ij} is the influence coefficient, i.e., the deflection in the direction of u_i due to a unit force applied in the direction of u_j. Combining Eqs. (3) to (5), one obtains

$$C_{ij} = \frac{\partial u_i}{\partial P_j} = \frac{\partial^2}{\partial P_i \partial P_j} \int_{A_f} J \, dA_f. \qquad (6)$$

Equation (6) gives the compliance factors as functions of the strain energy release rate. The energy release rate is a function of the stress intensity factors. The stress intensity factors for all modes of fractures[22] are given by the expression

$$J = \frac{1}{E'}\left[\left(\sum_{n=1}^{2} K_{In}\right)^2 + \left(\sum_{n=1}^{2} K_{IIn}\right)^2 + k\left(\sum_{n=1}^{2} K_{IIIn}\right)^2\right], \quad (7)$$

where $k = 1 + v$, v is the Poisson's ratio, $E' = E/(1-v)$ for plain strain condition, and E is Young's modulus.

For the open mode of the crack of the beam, Eq. (7) can be rewritten as

$$J = \frac{1}{E'}(K_{I1} + K_{I2})^2. \qquad (8)$$

The expressions for stress intensity factors from earlier studies[22] are

$$K_{I1} = \frac{P_1}{BW}\sqrt{\pi a}\left(F_1\left(\frac{a}{W}\right)\right); \qquad (9)$$

$$K_{I2} = \frac{6P_2}{BW^2}\sqrt{\pi a}\left(F_2\left(\frac{a}{W}\right)\right), \qquad (10)$$

where the functions F_1 and F_2 are given by[22]

$$F_1\left(\frac{a}{W}\right) = \sqrt{\frac{2W}{\pi a}\tan\left(\frac{\pi a}{2W}\right)}$$

$$\times \frac{0.752 + 2.02(a/W) + 0.37(1 - \sin(\pi a/2W))^3}{\cos(\pi a/2W)};$$

$$F_2\left(\frac{a}{W}\right) = \sqrt{\frac{2W}{\pi a}\tan\left(\frac{\pi a}{2W}\right)}\,\frac{0.923 + 0.199(1 - \sin(\pi a/2W))^4}{\cos(\pi a/2W)}.$$

For a beam with a surface crack of width B, the flexibility elements can be written as

$$C_{ij} = \frac{\partial u_i}{\partial P_j} = \frac{\partial^2}{\partial P_i \partial P_j}\int_{-B/2}^{B/2}\int_0^{a_1} J(a)\,da\,dz. \qquad (11)$$

Incorporating the value of the strain energy release rate J, Eq. (8), and stress intensity factors K_{I1} and K_{I2}, Eq. (9) and (10), Eq. (11) can be modified as

$$C_{ij} = \frac{B}{E'}\frac{\partial^2}{\partial P_i \partial P_j}\int_0^{a_1}(K_{I1} + K_{I2})^2 \, da. \qquad (12)$$

Writing $\xi = (a/W)$, one obtains $d\xi = da/W$.

We get $da = W d\xi$ and when $a = 0$, $\xi = 0$, and when $a = a_1$, $\xi = a_1/W = \xi_1$.

From the above condition, Eq. (12) becomes

$$C_{ij} = \frac{BW}{E'}\frac{\partial^2}{\partial P_i \partial P_j}\int_0^{\xi_1}(K_{I1} + K_{I2})^2 d\xi. \qquad (13)$$

From Eq. (13), the influence coefficients $C_{11}, C_{12}(= C_{21})$, and C_{22} can be calculated as:

$$C_{11} = \frac{BW}{E'}\int_0^{\xi_1}\frac{\pi a}{B^2 W^2}2(F_I(\xi))^2 d\xi; \qquad (14)$$

$$C_{12} = C_{21} = \frac{12\pi}{E'BW}\int_0^{\xi_1}\xi F_1(\xi)F_2(\xi)\,d\xi = \frac{2\pi}{BE'}\int_0^{\xi_1}\xi(F_1(\xi))^2 d\xi; \qquad (15)$$

$$C_{22} = \frac{72\pi}{E'BW^2}\int_0^{\xi_1}\xi F_1(\xi)F_2(\xi)\,d\xi. \qquad (16)$$

In dimensionless form, the above equations, Eqs. (14) to (16), can be written as:

$$\bar{C}_{11} = C_{11}\frac{BE'}{2\pi}; \qquad (17)$$

$$\bar{C}_{12} = \bar{C}_{21} = C_{12}\frac{E'BW}{12\pi}; \qquad (18)$$

$$\bar{C}_{22} = C_{22}\frac{E'BW^2}{72\pi}. \qquad (19)$$

The local stiffness matrix can be obtained by taking the inverse of the compliance matrix.

$$K = \begin{bmatrix} K_{11} & K_{12} \\ K_{21} & K_{22} \end{bmatrix} = \begin{bmatrix} C_{11} & C_{12} \\ C_{21} & C_{22} \end{bmatrix}^{-1}.$$

The stiffness matrix for the position of first and second crack can be obtained as follows:

$$K' = \begin{bmatrix} K'_{11} & K'_{12} \\ K'_{21} & K'_{22} \end{bmatrix} = \begin{bmatrix} C'_{11} & C'_{12} \\ C'_{21} & C'_{22} \end{bmatrix}^{-1} \qquad (20a)$$

and

$$K'' = \begin{bmatrix} K''_{11} & K''_{12} \\ K''_{21} & K''_{22} \end{bmatrix} = \begin{bmatrix} C''_{11} & C''_{12} \\ C''_{21} & C''_{22} \end{bmatrix}^{-1}. \qquad (20b)$$
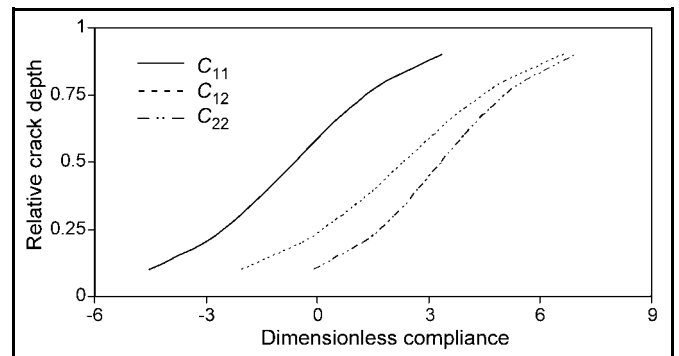

Figure 2. Relative crack depth vs. dimensionless compliance.

The dependence of the crack depth on the dimensionless compliance is shown in Fig. 2 for three values of compliance factor.

3. ANALYSIS OF VIBRATION CHARACTERISTICS OF THE CRACKED BEAM

3.1. Free Vibration

A cantilever beam of length L, width B, and depth W with crack depth a_1 at a distance L_1 and crack depth a_2 at a distance L_2 from the fixed end is considered (shown in Fig. 1). The system is described by equations for longitudinal and transverse vibration[23]

$$\frac{\partial^2 u}{\partial x^2} = \frac{1}{c_u^2}\frac{\partial^2 u}{\partial t^2} \text{ and } -\frac{\partial^4 y}{\partial x^4} = \frac{1}{c_y^2}\frac{\partial^2 y}{\partial t^2}, \qquad (21)$$

where $c_u = (E/\rho)^{1/2}$ and $c_y = (EI/\mu)^{1/2}$.

Here, $u_1(x,t), u_2(x,t)$, and $u_3(x,t)$ are longitudinal vibrations for the sections before and after the cracks. Moreover, $y_1(x,t), y_2(x,t)$, and $y_3(x,t)$ are bending vibrations for the same sections (shown in Fig. 3).
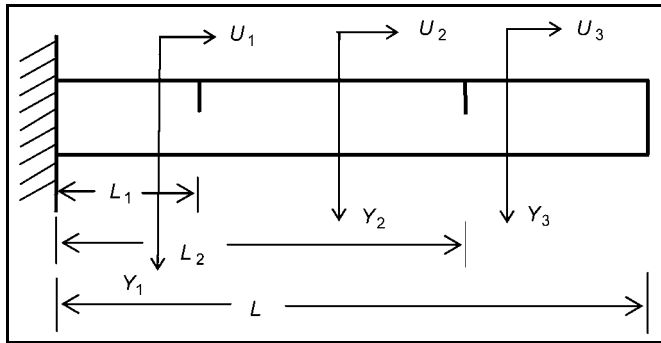
Figure 3. Beam model with cracks.

If T is the period of vibration, Eq. (21) can be written in nondimensional form as

$$\frac{\partial^2 \bar{u}}{\partial \bar{x}^2} = \frac{1}{c_{\bar{u}}^2}\frac{\partial^2 \bar{u}}{\partial \bar{t}^2} \text{ and } -\frac{\partial^4 \bar{y}}{\partial \bar{x}^4} = \frac{1}{c_{\bar{y}}^2}\frac{\partial^2 \bar{y}}{\partial \bar{t}^2}, \qquad (22)$$

where

$$\bar{x} = \frac{x}{L}; \ \bar{u} = \frac{u}{L}; \ \bar{y} = \frac{y}{L}; \ \bar{t} = \frac{t}{T}; \ \beta_1 = \frac{L_1}{L}; \ \beta_2 = \frac{L_2}{L}.$$

The normal functions for the system (22) are[23]

$$\bar{u}_1(\bar{x}) = A_1\cos(\bar{k}_u\bar{x}) + A_2\sin(\bar{k}_u\bar{x}); \qquad (23a)$$

$$\bar{u}_2(\bar{x}) = A_3\cos(\bar{k}_u\bar{x}) + A_4\sin(\bar{k}_u\bar{x}); \qquad (23b)$$

$$\bar{u}_3(\bar{x}) = A_5\cos(\bar{k}_u\bar{x}) + A_6\sin(\bar{k}_u\bar{x}); \qquad (23c)$$

$$\bar{y}_1(\bar{x}) = A_7\cosh(\bar{k}_y\bar{x}) + A_8\sinh(\bar{k}_y\bar{x}) + A_9\cos(\bar{k}_y\bar{x}) + A_{10}\sin(\bar{k}_y\bar{x}); \qquad (23d)$$

$$\bar{y}_2(\bar{x}) = A_{11}\cosh(\bar{k}_y\bar{x}) + A_{12}\sinh(\bar{k}_y\bar{x}) + A_{13}\cos(\bar{k}_y\bar{x}) + A_{14}\sin(\bar{k}_y\bar{x}); \qquad (23e)$$

$$\bar{y}_3(\bar{x}) = A_{15}\cosh(\bar{k}_y\bar{x}) + A_{16}\sinh(\bar{k}_y\bar{x}) + A_{17}\cos(\bar{k}_y\bar{x}) + A_{18}\sin(\bar{k}_y\bar{x}), \qquad (23f)$$

where $\bar{k}_u = \frac{\omega L}{c_u}$, $\bar{k}_y = \left(\frac{\omega L^2}{c_y}\right)^{1/2}$, $\mu = A\rho$, $A_i\,(i = 1, 18)$ are the constants to be determined by the boundary conditions.

The associated boundary conditions for the cracked cantilever beam under consideration are: at the clamped end, the longitudinal deformation (24), the bending deflection (25), and slope of beam (26) are zero. At the free end, the longitudinal force (27), the vertical bending moment (28), and the shear force (29) are zero. At the crack section, the axial force before and after the crack (30) and (34), the lateral displacement (31) and (35), the bending moment (32) and (36), and the shear force (33) and (37) are same. To the left and right of the crack, we find discontinuity of axial deformations (38) and (40) and bending moments (39) and (41).

$$\bar{u}_1(0) = 0; \qquad (24)$$

$$\bar{y}_1(0) = 0; \qquad (25)$$

$$\bar{y}_1'(0) = 0; \qquad (26)$$

$$\bar{u}_3'(1) = 0; \qquad (27)$$

$$\bar{y}_3''(1) = 0; \qquad (28)$$

$$\bar{y}_3'''(1) = 0; \qquad (29)$$

$$\bar{u}_1'(\beta_1) = \bar{u}_2'(\beta_1); \qquad (30)$$

$$\bar{y}_1(\beta_1) = \bar{y}_2(\beta_1); \qquad (31)$$

$$\bar{y}_1''(\beta_1) = \bar{y}_2''(\beta_1); \qquad (32)$$

$$\bar{y}_1'''(\beta_1) = \bar{y}_2'''(\beta_1); \qquad (33)$$

$$\bar{u}_2'(\beta_2) = \bar{u}_3'(\beta_2); \qquad (34)$$

$$\bar{y}_2(\beta_2) = \bar{y}_3(\beta_2); \qquad (35)$$

$$\bar{y}_2''(\beta_2) = \bar{y}_3''(\beta_2); \qquad (36)$$

$$\bar{y}_2'''(\beta_2) = \bar{y}_3'''(\beta_2); \qquad (37)$$

$$M_1M_2\bar{u}_1'(\beta_1) = M_2(\bar{u}_2(\beta_1) - \bar{u}_1(\beta_1)) + M_1(\bar{y}_2'(\beta_1) - \bar{y}_1'(\beta_1)); \qquad (38)$$

$$M_3M_4\bar{y}_1''(\beta_1) = M_4(\bar{y}_2'(\beta_1) - \bar{y}_1'(\beta_1)) + M_3(\bar{u}_2(\beta_1) - \bar{u}_1(\beta_1)); \qquad (39)$$

$$M_5M_6\bar{u}_2'(\beta_2) = M_6(\bar{u}_3(\beta_2) - \bar{u}_2(\beta_2)) + M_5(\bar{y}_3'(\beta_2) - \bar{y}_2'(\beta_2)); \qquad (40)$$

$$M_7M_8\bar{y}_2''(\beta_2) = M_8(\bar{y}_3'(\beta_2) - \bar{y}_2'(\beta_2)) + M_7(\bar{u}_3(\beta_2) - \bar{u}_2(\beta_2)), \qquad (41)$$

where

$$M_1 = \frac{AE}{LK_{11}'}; \ M_2 = \frac{AE}{K_{12}'}; \ M_3 = \frac{EI}{LK_{22}'}; \ M_4 = \frac{EI}{L^2K_{21}'};$$

$$M_5 = \frac{AE}{LK_{11}''}; \ M_6 = \frac{AE}{K_{12}''}; \ M_7 = \frac{EI}{LK_{22}''}; \ M_8 = \frac{EI}{L^2K_{21}''}.$$

The normal functions given in Eqs. (23) along with the boundary conditions assumed in Eq. (24) through Eq. (41) yield the characteristic equation of the system as:

$$|Q| = 0, \qquad (42)$$

where

$$[Q] = \begin{bmatrix} 0 & 0 & 0 & 0 & 0 & 0 & 0 & 0 & 0 & 0 & 0 & 0 & 1 & 0 & 0 & 0 & 0 & 0 \\ 1 & 0 & 1 & 0 & 0 & 0 & 0 & 0 & 0 & 0 & 0 & 0 & 0 & 0 & 0 & 0 & 0 & 0 \\ 0 & 1 & 0 & 1 & 0 & 0 & 0 & 0 & 0 & 0 & 0 & 0 & 0 & 0 & 0 & 0 & 0 & 0 \\ 0 & 0 & 0 & 0 & 0 & 0 & 0 & 0 & 0 & 0 & 0 & 0 & 0 & 0 & 0 & 0 & -T_1 & -T_2 \\ 0 & 0 & 0 & 0 & 0 & 0 & 0 & 0 & G_3 & G_4 & -G_7 & -G_8 & 0 & 0 & 0 & 0 & 0 & 0 \\ 0 & 0 & 0 & 0 & 0 & 0 & 0 & 0 & G_4 & G_3 & G_8 & -G_7 & 0 & 0 & 0 & 0 & 0 & 0 \\ 0 & 0 & 0 & 0 & 0 & 0 & 0 & 0 & 0 & 0 & 0 & 0 & -T_6 & T_5 & T_6 & -T_5 & 0 & 0 \\ G_1 & G_2 & G_5 & G_6 & -G_1 & -G_2 & -G_5 & -G_6 & 0 & 0 & 0 & 0 & 0 & 0 & 0 & 0 & 0 & 0 \\ G_1 & G_2 & -G_5 & -G_6 & -G_1 & -G_2 & G_5 & G_6 & 0 & 0 & 0 & 0 & 0 & 0 & 0 & 0 & 0 & 0 \\ G_2 & G_1 & G_6 & -G_5 & -G_2 & -G_1 & -G_6 & G_5 & 0 & 0 & 0 & 0 & 0 & 0 & 0 & 0 & 0 & 0 \\ 0 & 0 & 0 & 0 & 0 & 0 & 0 & 0 & 0 & 0 & 0 & 0 & 0 & 0 & -T_4 & T_3 & T_4 & -T_3 \\ 0 & 0 & 0 & 0 & G_9 & G_{10} & G_{11} & G_{12} & -G_9 & -G_{10} & -G_{11} & -G_{12} & 0 & 0 & 0 & 0 & 0 & 0 \\ 0 & 0 & 0 & 0 & G_9 & G_{10} & -G_{11} & -G_{12} & -G_9 & -G_{10} & G_{11} & G_{12} & 0 & 0 & 0 & 0 & 0 & 0 \\ 0 & 0 & 0 & 0 & G_{10} & G_9 & G_{12} & -G_{11} & -G_{10} & -G_9 & -G_{12} & G_{11} & 0 & 0 & 0 & 0 & 0 & 0 \\ -S_3 & -S_4 & S_5 & -S_6 & S_3 & S_4 & -S_5 & S_6 & 0 & 0 & 0 & 0 & S_1 & -S_2 & T_5 & T_6 & 0 & 0 \\ S_7 & S_8 & -S_9 & -S_{10} & -S_{11} & -S_{12} & S_{13} & -S_{14} & 0 & 0 & 0 & 0 & S_{15} & S_{16} & -S_{15} & -S_{16} & 0 & 0 \\ 0 & 0 & 0 & 0 & V_3 & V_4 & -V_5 & V_6 & -V_3 & -V_4 & V_5 & -V_6 & 0 & 0 & V_1 & V_2 & -T_3 & -T_4 \\ 0 & 0 & 0 & 0 & V_7 & V_8 & -V_9 & -V_{10} & -V_{11} & -V_{12} & V_{13} & -V_{14} & 0 & 0 & V_{15} & V_{16} & -V_{15} & -V_{16} \end{bmatrix},$$

where

$$T_1 = \sin \bar{k}_u; \quad T_2 = \cos \bar{k}_u; \quad T_3 = \cos(\bar{k}_u \gamma);$$

$$T_4 = \sin(\bar{k}_u \gamma); \quad T_5 = \cos(\bar{k}_u \beta); \quad T_6 = \sin(\bar{k}_u \beta);$$

$$G_1 = \cosh(\bar{k}_y \beta); \quad G_2 = \sinh(\bar{k}_y \beta); \quad G_3 = \cosh(\bar{k}_y);$$

$$G_4 = \sinh(\bar{k}_y); \quad G_5 = \cos(\bar{k}_y \beta); \quad G_6 = \sin(\bar{k}_y \beta);$$

$$G_7 = \cos(\bar{k}_y); \quad G_8 = \sin(\bar{k}_y); \quad G_9 = \cosh(\bar{k}_y \gamma);$$

$$G_{10} = \sinh(\bar{k}_y \gamma); \quad G_{11} = \cos(\bar{k}_y \gamma); \quad G_{12} = \sin(\bar{k}_y \gamma);$$

$$M_1 = \frac{AE}{Lk'_{11}}; \quad M_2 = \frac{AE}{k'_{12}}; \quad M_3 = \frac{EI}{Lk'_{22}}; \quad M_4 = \frac{EI}{L^2 k'_{21}};$$

$$M_{12} = M_1/M_2; \quad M_{34} = M_3/M_4;$$

$$S_1 = T_5 - M_1 \bar{k}_u T_6; \quad S_2 = T_6 + M_1 \bar{k}_u T_5; \quad S_3 = M_{12} \bar{k}_y G_2;$$

$$S_4 = M_{12} \bar{k}_y G_1; \quad S_5 = M_{12} \bar{k}_y G_6; \quad S_6 = M_{12} \bar{k}_y G_5;$$

$$S_7 = M_3 \bar{k}_y^2 G_1 + \bar{k}_y G_2; \quad S_8 = M_3 \bar{k}_y^2 G_2 + \bar{k}_y G_1;$$

$$S_9 = M_3 \bar{k}_y^2 G_5 + \bar{k}_y G_6; \quad S_{10} = M_3 \bar{k}_y^2 G_6 - \bar{k}_y G_5;$$

$$S_{11} = \bar{k}_y G_2; \quad S_{12} = \bar{k}_y G_1; \quad S_{13} = \bar{k}_y G_6;$$

$$S_{14} = \bar{k}_y G_5; \quad S_{15} = M_{34} T_5; \quad S_{16} = M_{34} T_6;$$

$$M_5 = \frac{AE}{Lk''_{22}}; \quad M_6 = \frac{AE}{k''_{23}}; \quad M_7 = \frac{EI}{Lk''_{33}}; \quad M_8 = \frac{EI}{L^2 K''_{32}};$$

$$M_{56} = M_5/M_6; \quad M_{78} = M_7/M_8;$$

$$V_1 = T_3 - M_5 \bar{k}_u T_4; \quad V_2 = T_4 + M_5 \bar{k}_u T_3; \quad V_3 = M_{56} \bar{k}_y G_{10};$$

$$V_4 = M_{56} \bar{k}_y G_9; \quad V_5 = M_{56} \bar{k}_y G_{12}; \quad V_6 = M_{56} \bar{k}_y G_{11};$$

$$V_7 = M_7 \bar{k}_y^2 G_9 + \bar{k}_y G_{10}; \quad V_8 = M_7 \bar{k}_y^2 G_{10} + \bar{k}_y G_9;$$

$$V_9 = M_7 \bar{k}_y^2 G_{11} + \bar{k}_y G_{12}; \quad V_{10} = M_7 \bar{k}_y^2 G_{12} - \bar{k}_y G_{11};$$

$$V_{11} = \bar{k}_y G_{10}; \quad V_{12} = \bar{k}_y G_9; \quad V_{13} = \bar{k}_y G_{12};$$

$$V_{14} = \bar{k}_y G_{11}; \quad V_{15} = M_{78} T_3; \quad V_{16} = M_{78} T_4,$$

where $|Q|$ is a function of the natural circular frequency ω, the relative crack locations β_1 and β_2, and the local stiffness matrices K' and K'', which in turn are functions of the relative crack depths.

3.2. Forced Vibration

If the cantilever beam with transverse cracks is excited at its free end by a harmonic excitation $(Y = Y_0 \sin \omega t)$, the non-dimensional amplitude at the free end may be expressed as $\bar{y}_3(1) = y_0/L = \bar{y}_0$. Therefore, the boundary conditions for the beam remain the same as before except in the case of the expression Eq. (29), which is changed to $\bar{y}_3(1) = \bar{y}_0$.

The constants $A_i (i = 1, 18)$ are computed from the algebraic condition $Q_1 D = B_1$, where Q_1 is the (18×18) matrix obtained from the boundary conditions as mentioned before, D is a column matrix obtained from the constants, and B_1 is a column matrix whose transpose is given by

$$B_1^T = [0 \; 0 \; 0 \; \bar{y}_0 \; 0 \; 0 \; 0 \; 0 \; 0 \; 0 \; 0 \; 0 \; 0 \; 0 \; 0 \; 0 \; 0 \; 0].$$

4. NUMERICAL ANALYSIS

An aluminium cantilever beam with a uniform cross-section area of length 80 cm, breadth 5 cm, depth 6 mm, modulus of elasticity $E = 0.724 \times 10^{11}$ N/m², Poison's ratio $v = 0.334$, and density $\rho = 2713$ kg/m³ is considered for numerical analysis. The cracks are situated at two different positions $(L_1/L = 0.125, L_2/L = 0.25)$. The crack depths are chosen such that $a_{1,2}/W = 0.001, 0.1667, 0.334,$ and 0.5. The first, second, and third natural frequencies corresponding to various crack conditions are calculated. The fundamental mode shapes for longitudinal and transverse vibration of cracked and uncracked beams are plotted and compared. The transverse and longitudinal mode shapes for the beams are plotted for beam position (x) in cm vs. relative amplitude $(\bar{u})$ and $(\bar{y})$ respectively. The magnified view of the mode shapes is also plotted for the elastic cantilever beams in the vicinity of the crack in order to observe the change in the mode shape.

Similarly, results are obtained for a mild steel beam having the same geometry as an aluminium beam. The mild steel beam specimen has a modulus of elasticity $E = 2.1 \times 10^{11}$ N/m², Poison's ratio $v = 0.3$, and density $\rho = 7860$ kg/m³. The numerical results are shown in Figs. 4-32.
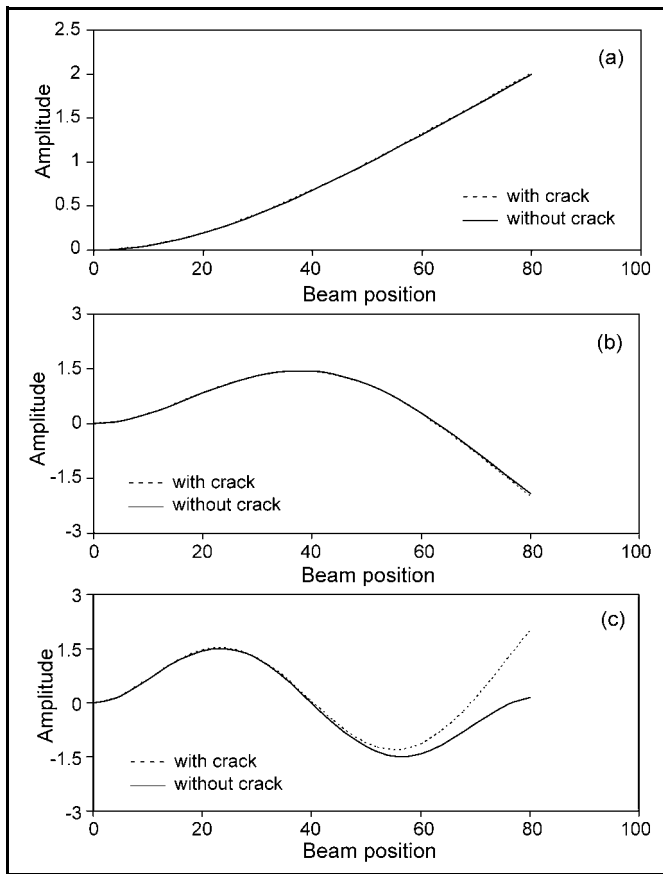
Figure 4. Transverse vibration ($\xi_1 = 0.1667$, $\beta_1 = 0.125$). (a) First mode; (b) second mode; (c) third mode.
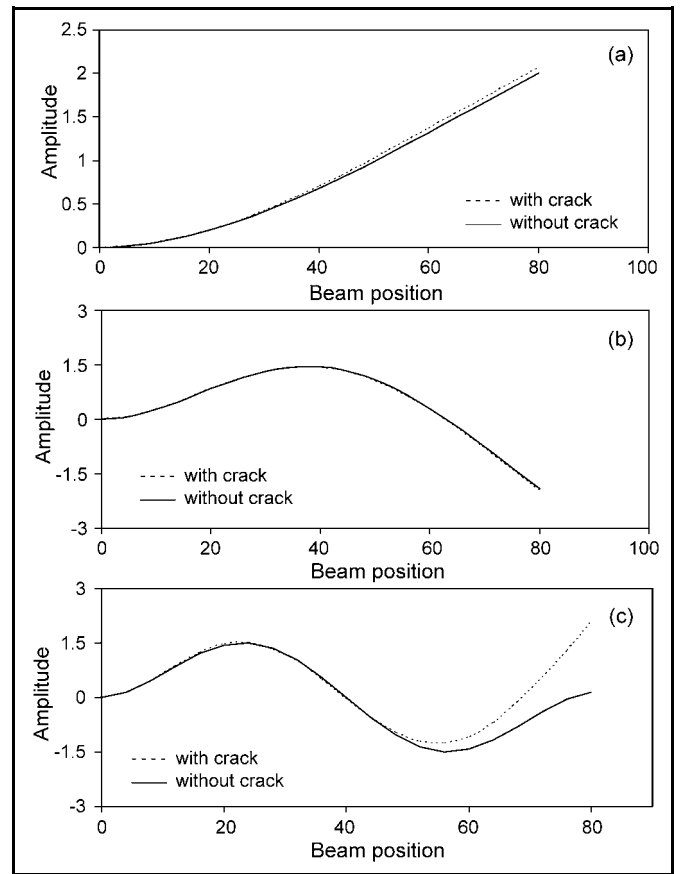

Figure 6. Transverse vibration ($\xi_1 = 0.5$, $\beta_1 = 0.125$). (a) First mode; (b) second mode; (c) third mode.
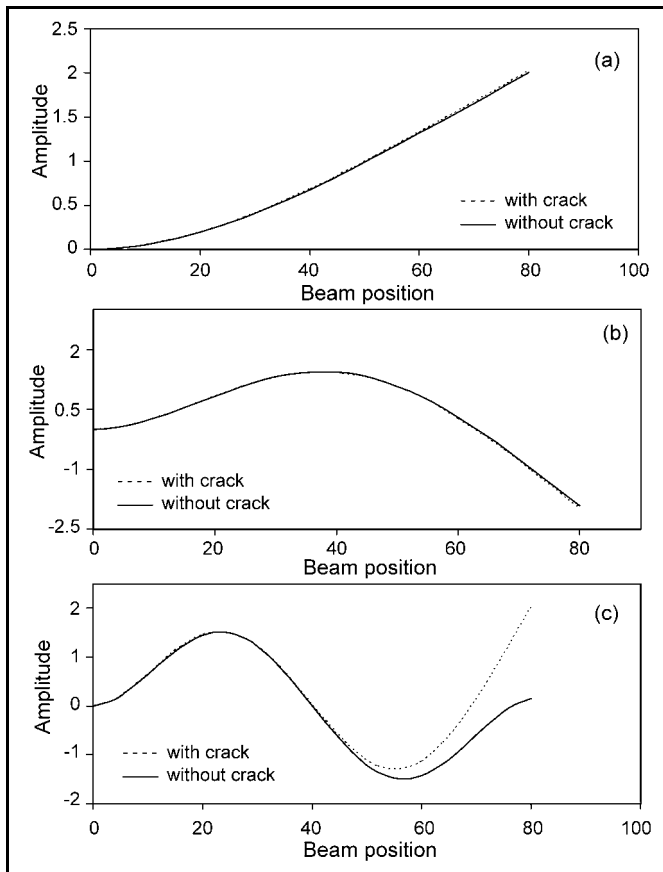

Figure 5. Transverse vibration ($\xi_1 = 0.334$, $\beta_1 = 0.125$). (a) First mode; (b) second mode; (c) third mode.
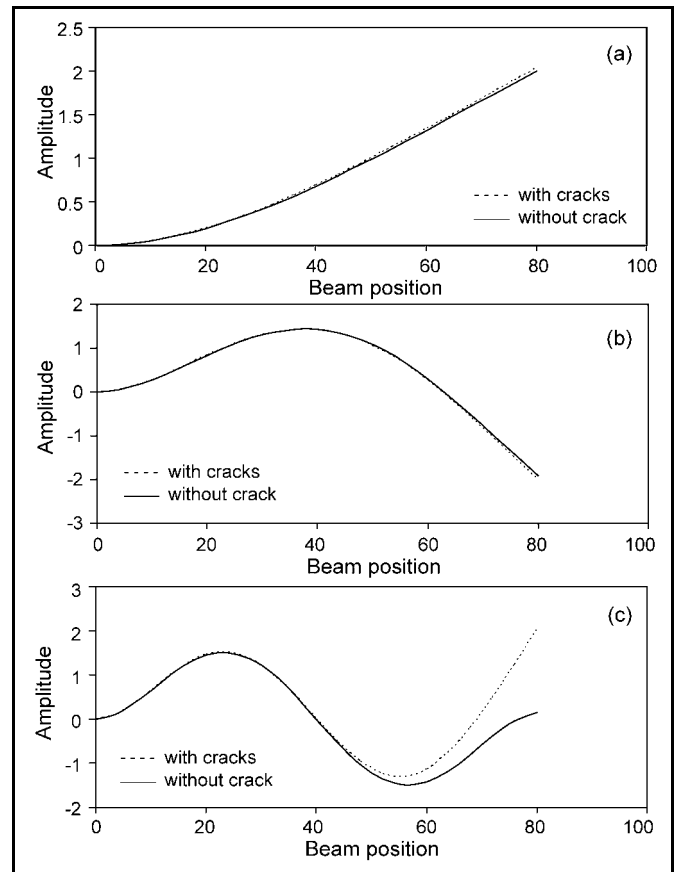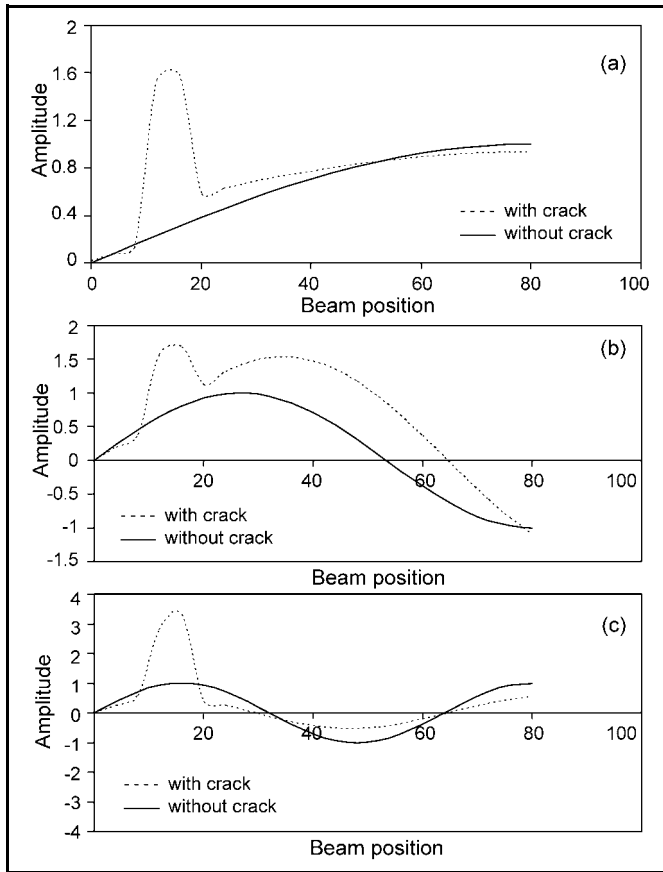

Figure 7. Transverse vibration ($\xi_1 = 0.1667$, $\xi_2 = 0.334$, $\beta_1 = 0.125$, $\beta_2 = 0.25$). (a) First mode; (b) second mode; (c) third mode.
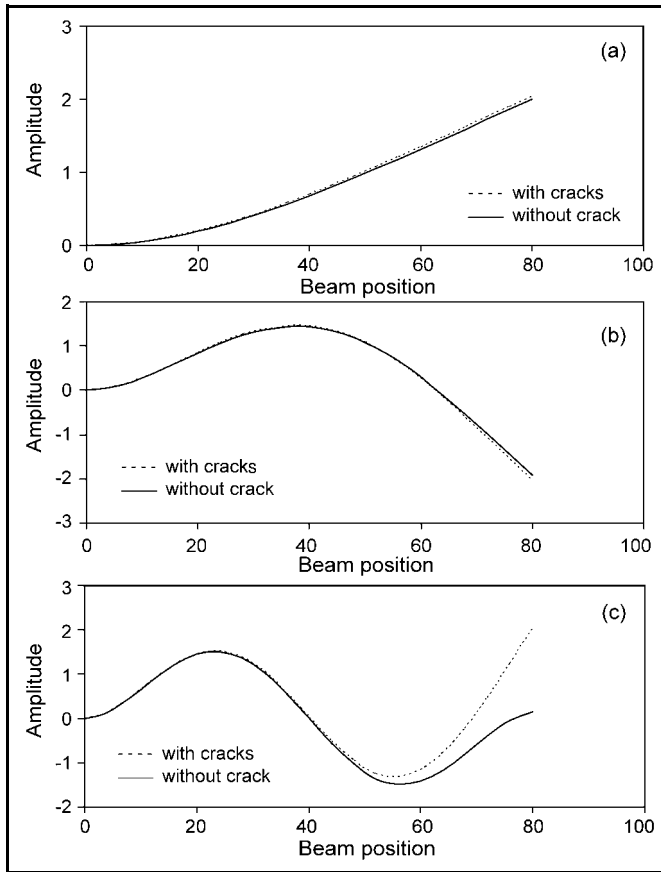
Figure 8. Transverse vibration ($\xi_1 = 0.334, \xi_2 = 0.1667, \beta_1 = 0.125, \beta_2 = 0.25$). (a) First mode; (b) second mode; (c) third mode.
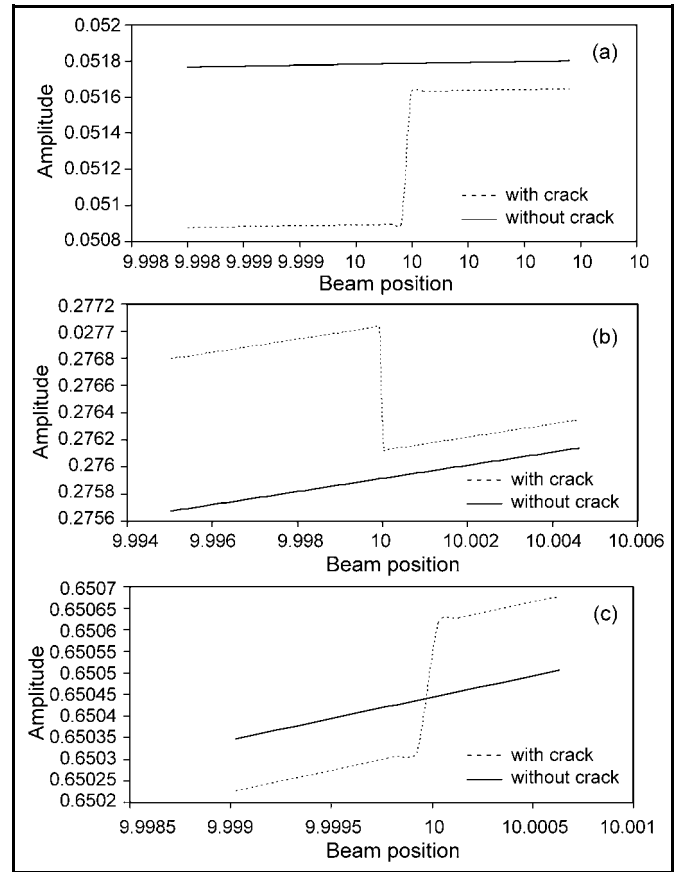

Figure 9. Transverse vibration ($\xi_1 = 0.334, \xi_2 = 0.334, \beta_1 = 0.125, \beta_2 = 0.25$). (a) First mode; (b) second mode; (c) third mode.
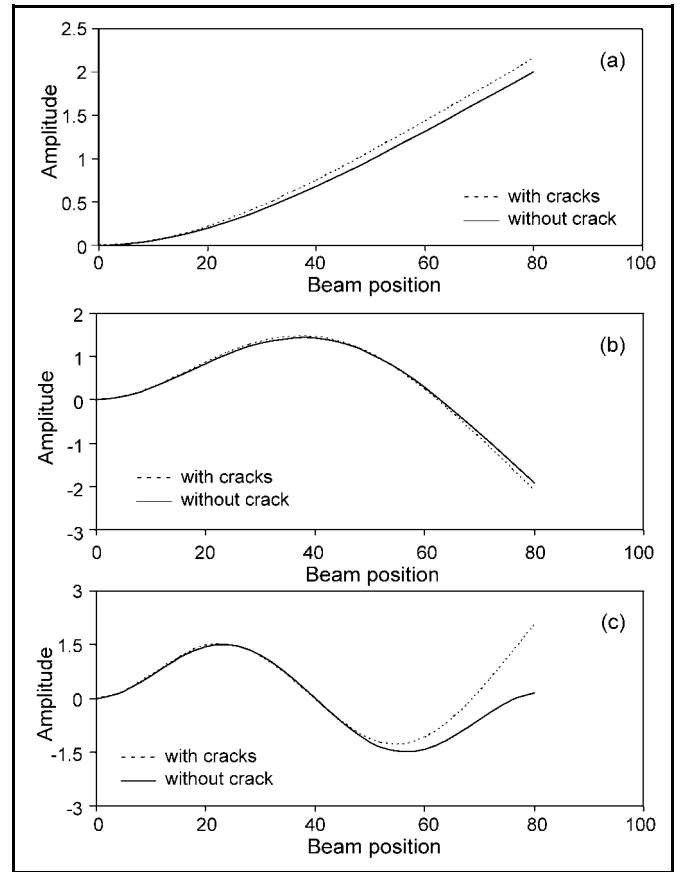
Figure 10. Transverse vibration ($\xi_1 = 0.5, \xi_2 = 0.5, \beta_1 = 0.125, \beta_2 = 0.25$). (a) First mode; (b) second mode; (c) third mode.
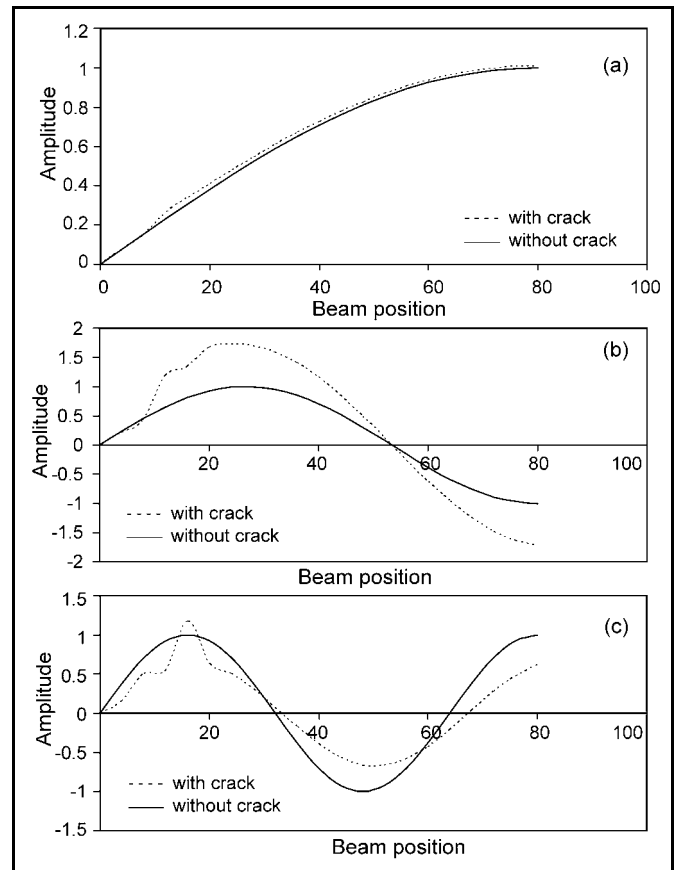
Figure 11. Longitudinal vibration ($\xi_1 = 0.5, \beta_1 = 0.125$). (a) First mode; (b) second mode; (c) third mode.

Figure 12. Longitudinal vibration ($\xi_1 = 0.5$, $\xi_2 = 0.5$, $\beta_1 = 0.125$, $\beta_2 = 0.25$). (a) First mode; (b) second mode; (c) third mode.

Figure 14. Magnified view of transverse vibration, aluminium beam ($\xi_1 = 0.1667$, $\beta_1 = 0.125$). (a) First mode; (b) second mode; (c) third mode.
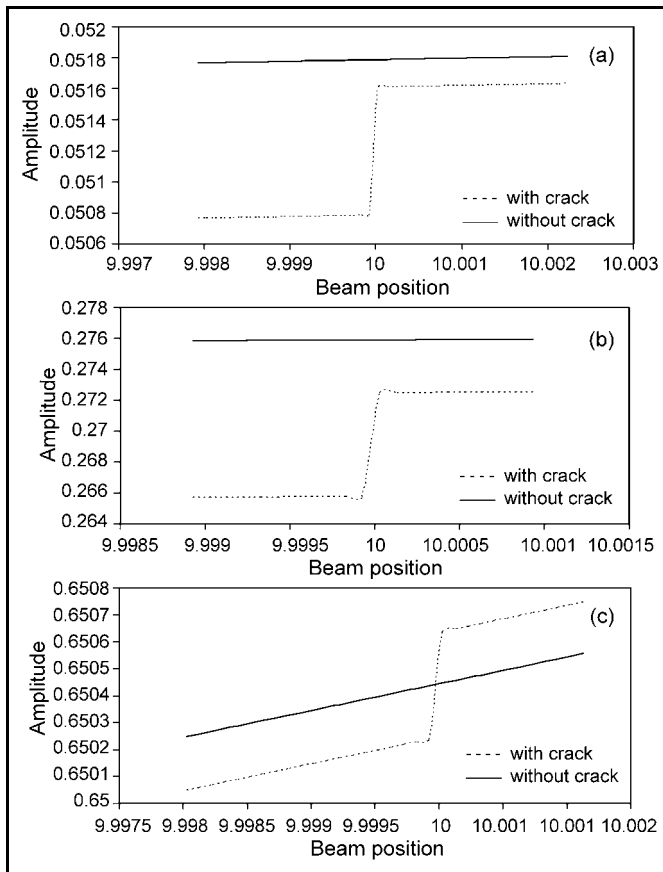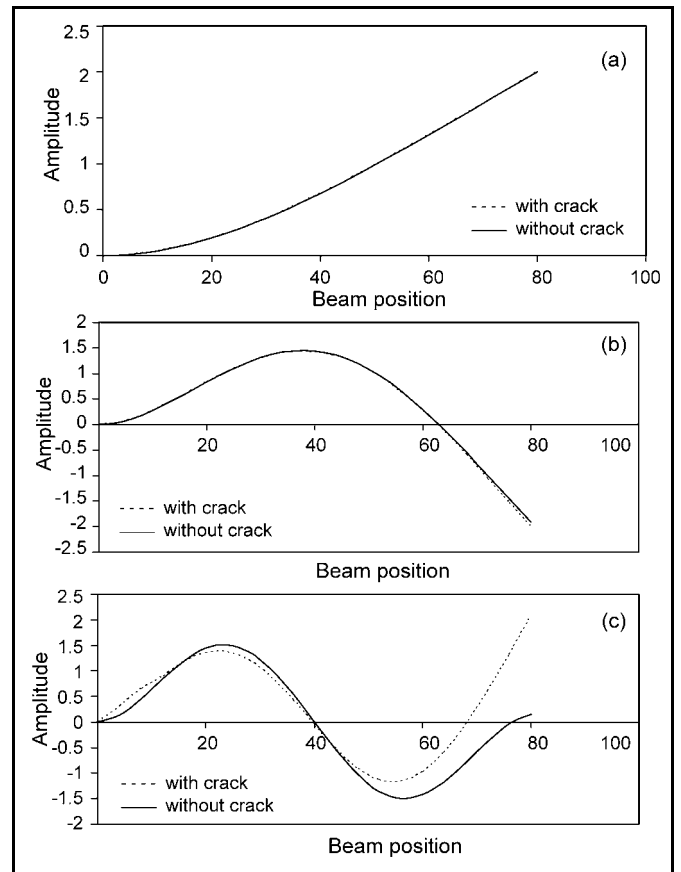

Figure 13. Magnified view of transverse vibration, aluminium beam ($\xi_1 = 0.01$, $\beta_1 = 0.125$). (a) First mode; (b) second mode; (c) third mode.

Figure 15. Transverse vibration, mild steel beam ($\xi_1 = 0.001$, $\beta_1 = 0.125$). (a) First mode; (b) second mode; (c) third mode.
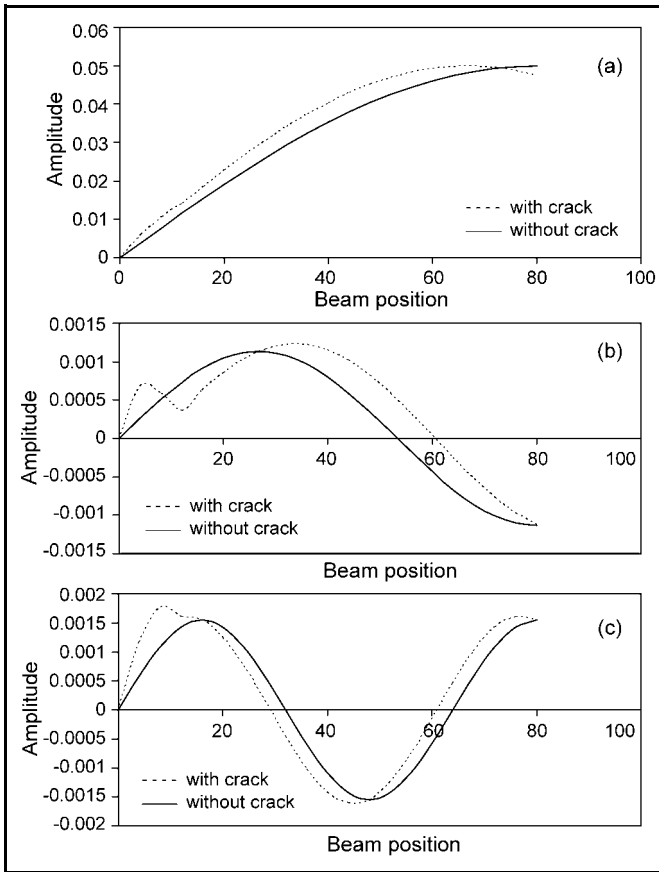
Figure 16. Longitudinal vibration, mild steel beam ($\xi_1 = 0.001$, $\beta_1 = 0.125$). (a) First mode; (b) second mode; (c) third mode.
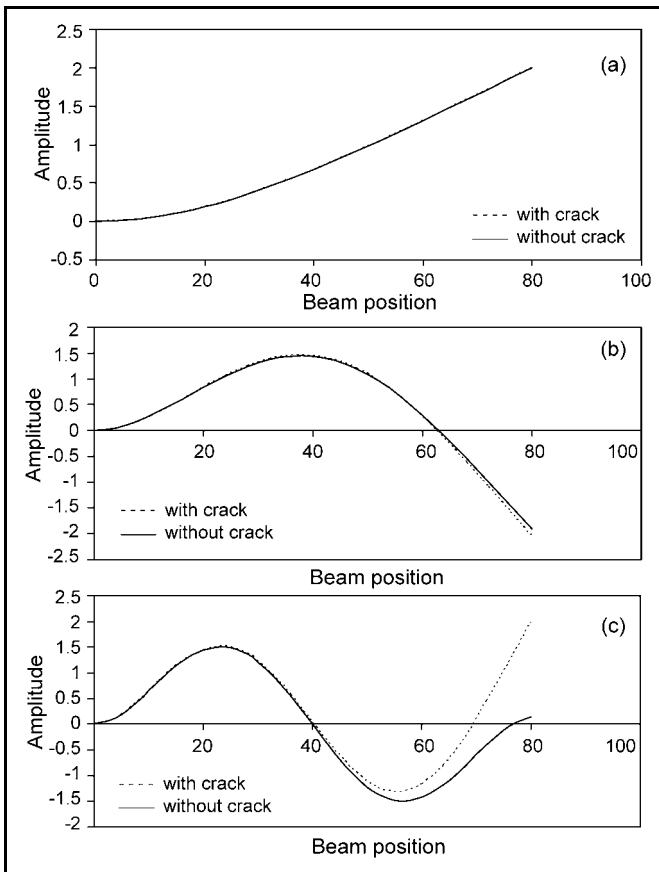

Figure 17. Transverse vibration, mild steel beam ($\xi_1 = 0.001$, $\xi_2 = 0.001$, $\beta_1 = 0.125$, $\beta_2 = 0.25$). (a) First mode; (b) second mode; (c) third mode.
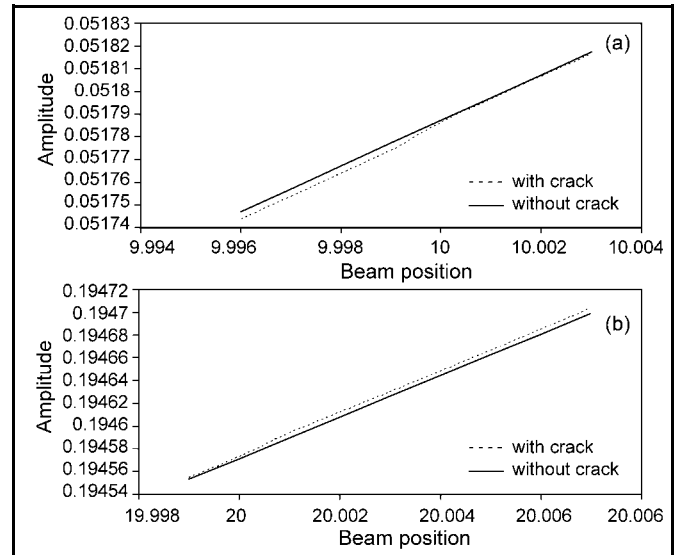

Figure 18. Magnified view of first mode of transverse vibration, mild steel beam ($\xi_1 = 0.001$, $\xi_2 = 0.001$). (a) $\beta_1 = 0.125$, (b) $\beta_2 = 0.25$.
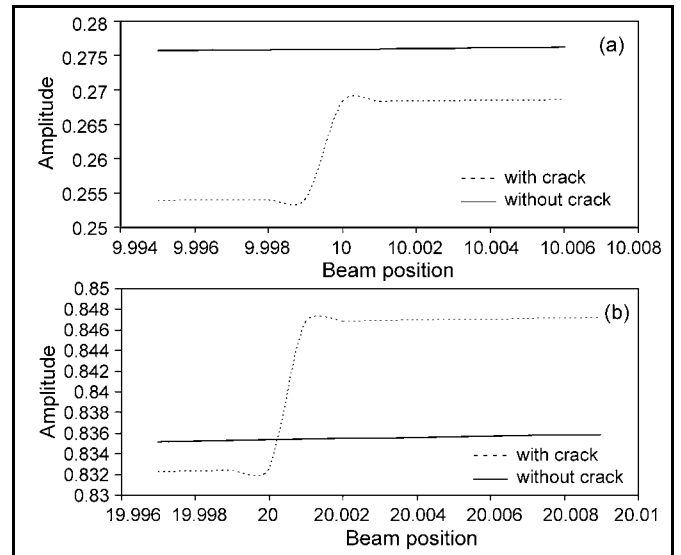

Figure 19. Magnified view of second mode of transverse vibration, mild steel beam ($\xi_1 = 0.001$, $\xi_2 = 0.001$). (a) $\beta_1 = 0.125$, (b) $\beta_2 = 0.25$.
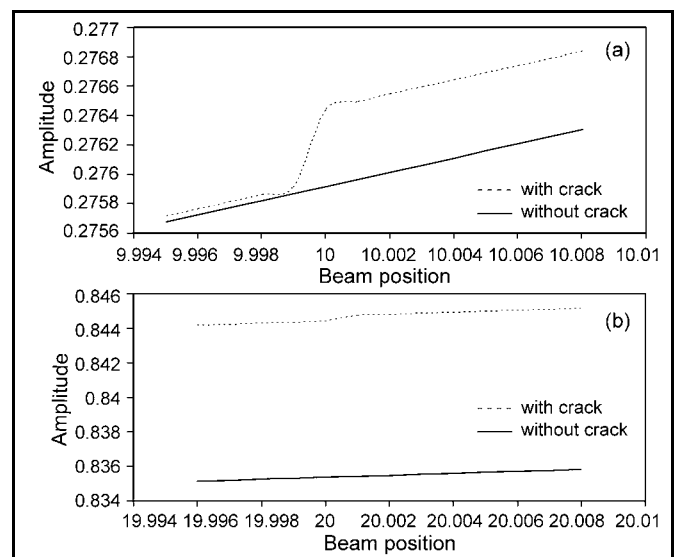

Figure 20. Magnified view of third mode of transverse vibration, mild steel beam ($\xi_1 = 0.001$, $\xi_2 = 0.001$). (a) $\beta_1 = 0.125$, (b) $\beta_2 = 0.25$.
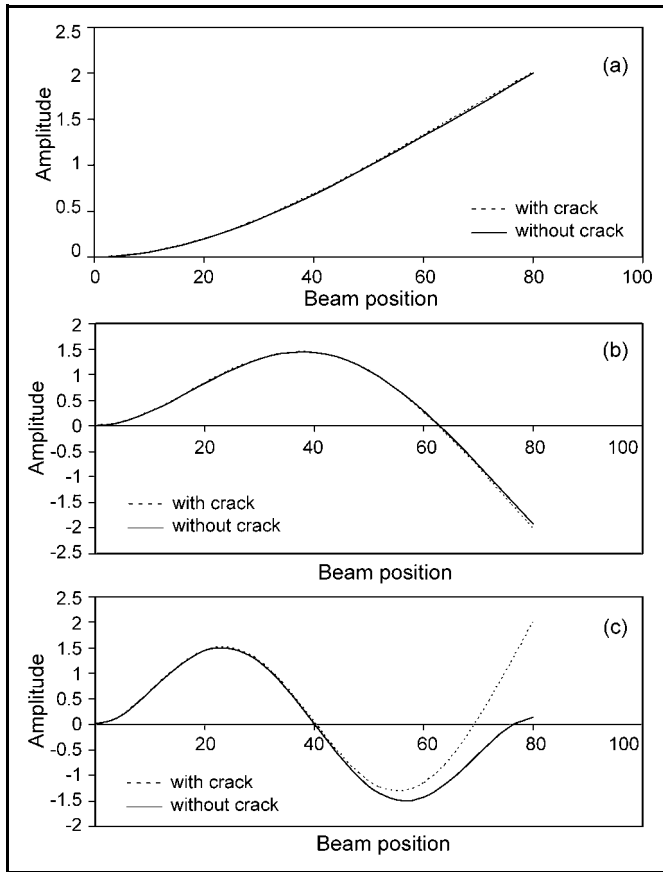
Figure 21. Transverse vibration, mild steel beam ($\xi_1 = 0.1667, \xi_2 = 0.1667$, $\beta_1 = 0.125$, $\beta_2 = 0.25$). (a) First mode; (b) second mode; (c) third mode.

Figure 22. Longitudinal vibration, mild steel beam ($\xi_1 = 0.001, \xi_2 = 0.001$, $\beta_1 = 0.125$, $\beta_2 = 0.25$). (a) First mode; (b) second mode; (c) third mode.

Figure 23. Longitudinal vibration, mild steel beam ($\xi_1 = 0.1667$, $\xi_2 = 0.1667$, $\beta_1 = 0.125$, $\beta_2 = 0.25$). (a) First mode; (b) second mode; (c) third mode.
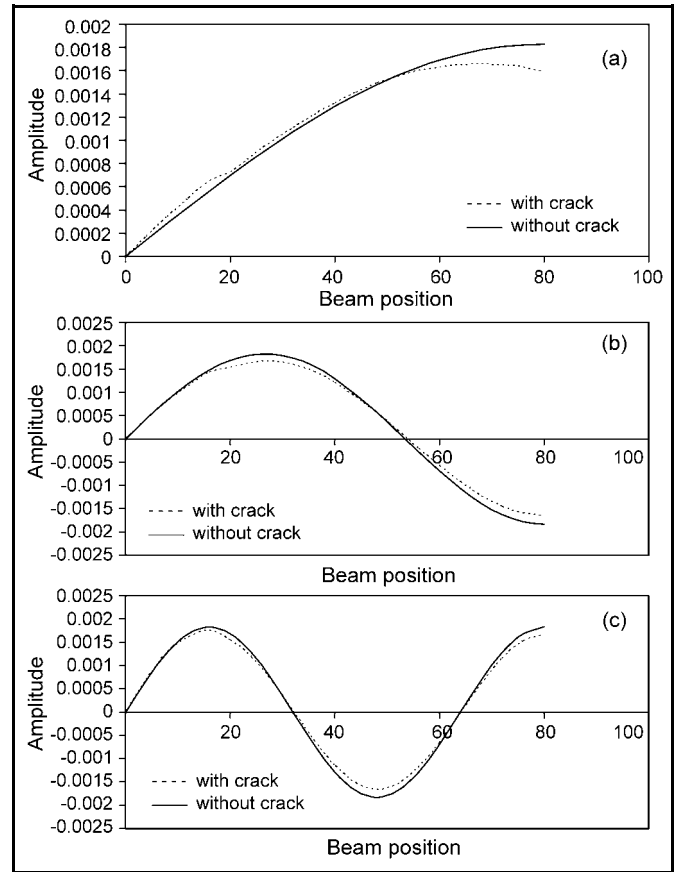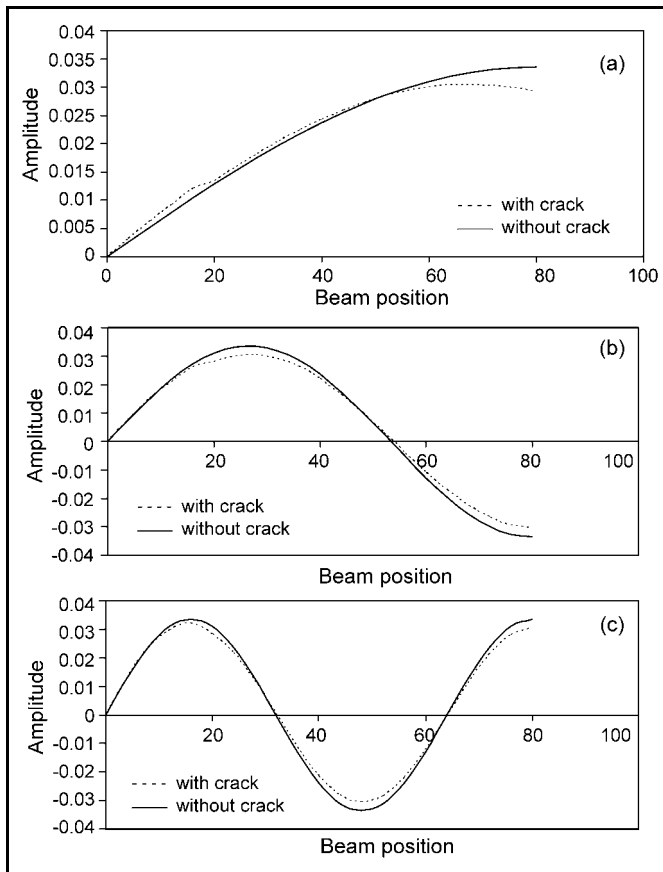
5. EXPERIMENTAL SET-UP

An experimental set-up shown in the schematic diagram (Fig. 33) was used for performing the experiments on aluminium and mild steel cantilever beam specimens. While conducting the experiment on the aluminium specimen, small mild steel foils (length 1 cm, width 1 cm, and thickness 0.05 cm) are adhered on the surface of beam. Ten foils are placed at 10 cm apart each on the aluminium beam. The specimen is set to vibrate under first, second, and third fundamental frequencies. A non-contact type of magnetic sensor (vibration pickup) was used to receive the signals at various positions where the foils are placed. The gap between the sensor and foil was kept as 0.2 cm. The signals obtained were fed to the vibration indicator through a power amplifier. The measured signals were used to plot the mode shapes for comparison with the theoretical results.

Similarly, experiments are performed on mild steel beam specimens. The experimental results for the aluminium beam are shown in Table 1.

6. DISCUSSION

The results obtained from the numerical analysis are presented in graphical forms.

The transverse vibration mode shapes for an aluminium beam with a single crack are shown in Figs. 4-6. In these figures, the relative crack depths considered are 0.1667, 0.334, and 0.5 respectively. However, the relative crack position was
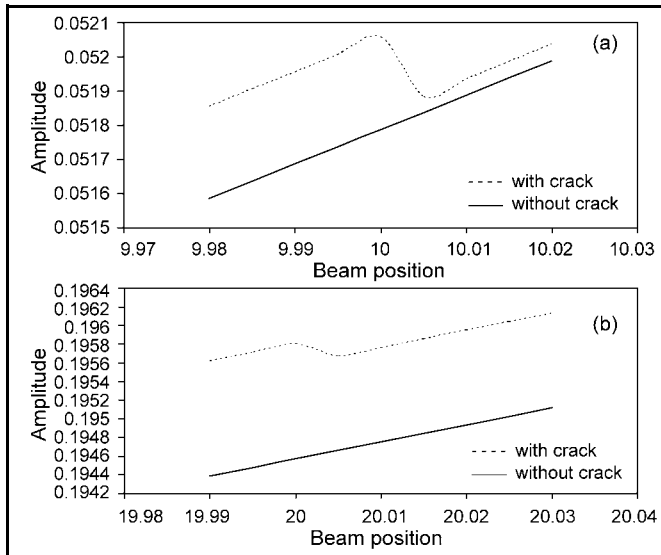
Figure 24. Magnified view of first mode of transverse vibration, mild steel beam ($\xi_1 = 0.1667$, $\xi_2 = 0.1667$). (a) $\beta_1 = 0.125$, (b) $\beta_2 = 0.25$.
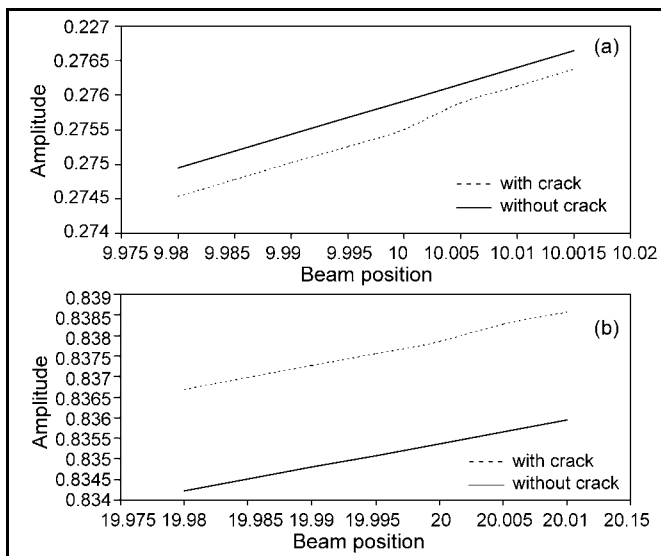

Figure 25. Magnified view of second mode of transverse vibration, mild steel beam ($\xi_1 = 0.1667$, $\xi_2 = 0.1667$). (a) $\beta_1 = 0.125$, (b) $\beta_2 = 0.25$.
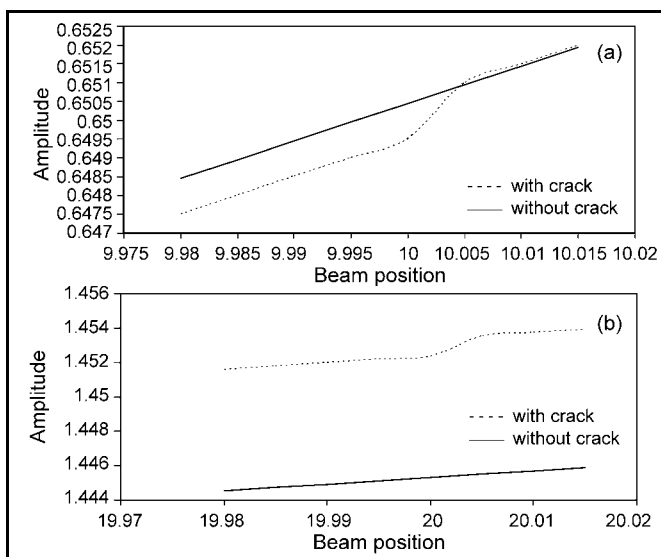

Figure 26. Magnified view of third mode of transverse vibration, mild steel beam ($\xi_1 = 0.1667$, $\xi_2 = 0.1667$). (a) $\beta_1 = 0.125$, (b) $\beta_2 = 0.25$.
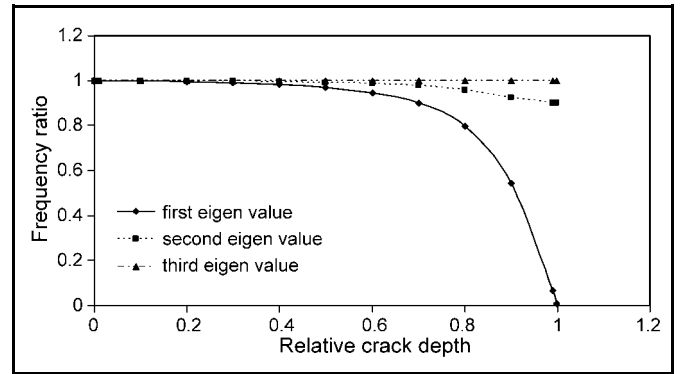
Figure 27. Variation of the eigen values of a mild steel cracked beam vs. the relative crack depth (ξ_1), $\beta_1 = 0.125$.

Figure 28. Variation of the eigen values of two cracked mild steel beam vs. the relative crack depth (ξ_2), $\xi_1 = 0.001$, $\beta_1 = 0.125$, $\beta_2 = 0.25$.

Figure 29. Variation of the eigen values of a cracked aluminium beam vs. the relative crack depth (ξ_1), $\beta_1 = 0.125$.
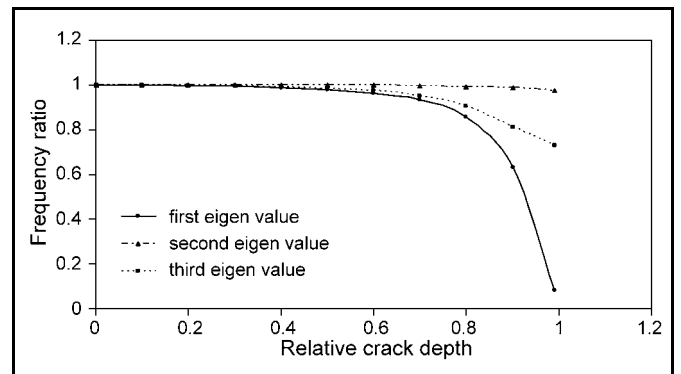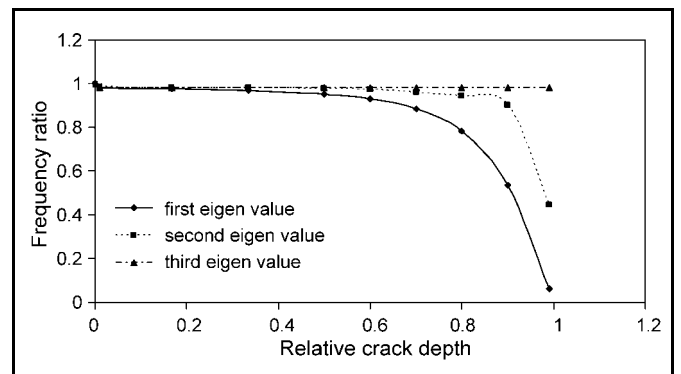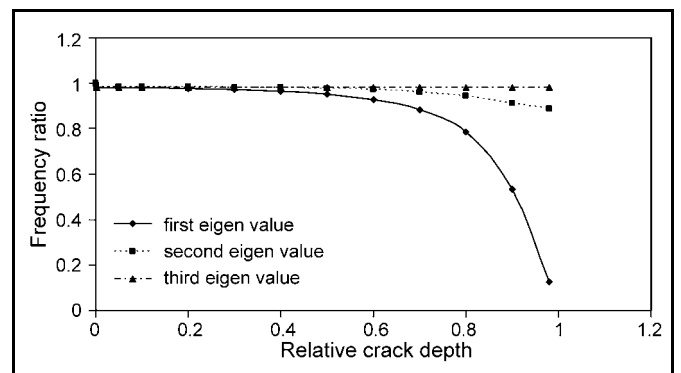

Figure 30. Variation of the eigen values of two cracked aluminium beam vs. the relative crack depth (ξ_1), $\xi_2 = 0.01$, $\beta_1 = 0.125$, $\beta_2 = 0.25$.
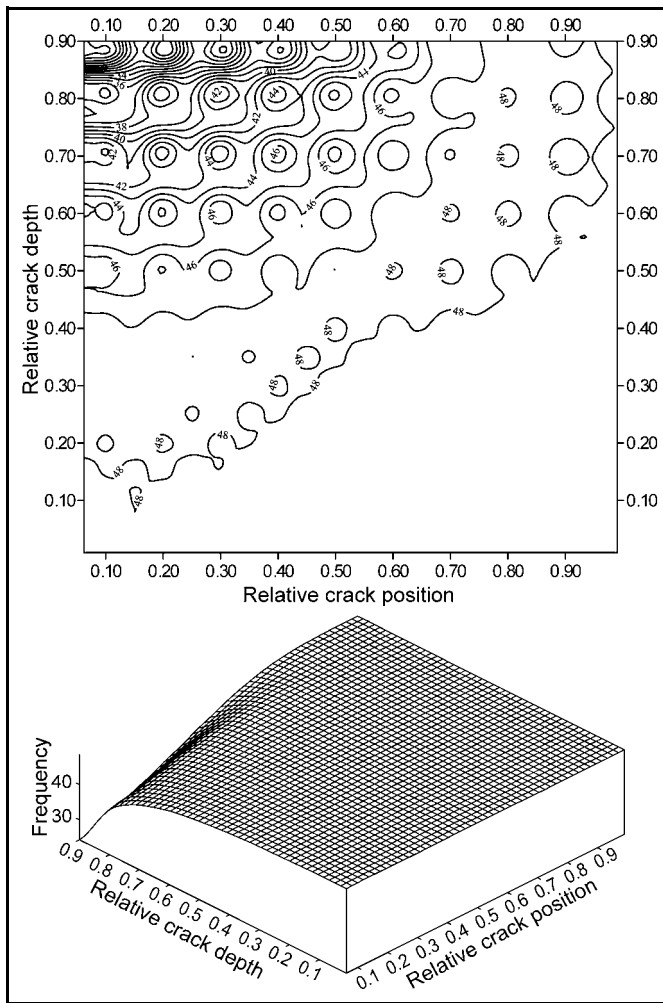
Figure 31. First fundamental frequencies of a cracked aluminium beam for various crack positions and depths. (a) Contours; (b) 3-D plot.

fixed at 0.125 for single crack analysis. For the two-crack beam vibration analysis, different combinations of relative crack depths were considered. Figures 7-10 show the transverse mode shapes for an aluminium beam with relative crack depths 0.1667, 0.334, and 0.5 respectively. For the same beam, the relative crack locations were chosen at 0.125 and 0.25.

The longitudinal mode shapes for a single deep crack $(a_1/W = 0.5)$ are shown in Fig 11. For deep two cracks $(a_1/W = a_2/W = 0.5)$, the results are shown in Fig. 12. For minute $(a_1/W = 0.001)$ and moderate cracks $(a_1/W = a_2/W = 0.1667)$, the magnified views of transverse mode shapes at the crack locations are depicted in Figs. 13 and 14.

Similar results, as discussed above, were obtained for the mild steel beam. The results are shown in Figs. 15-26. It is observed that there are no significant changes in transverse mode shapes for a minute crack $(a_1/W = a_2/W = 0.001)$ when compared with the same uncracked cantilever beam. For a moderate crack $(a_1/W = 0.1667)$, appreciable changes in mode shapes are noticed. For deep cracks $(a_1/W = a_2/W = 0.5)$, the change in mode shapes are quite substantial. However, remarkable changes are observed in longitudinal mode shapes at the crack positions even for a very small crack. Furthermore, the numerical results indicate that the deviation between the fundamental mode shapes of the cracked and uncracked beam is always sharply changed at the crack location. Such behaviours are noticed in the magnified views of the mode shapes.
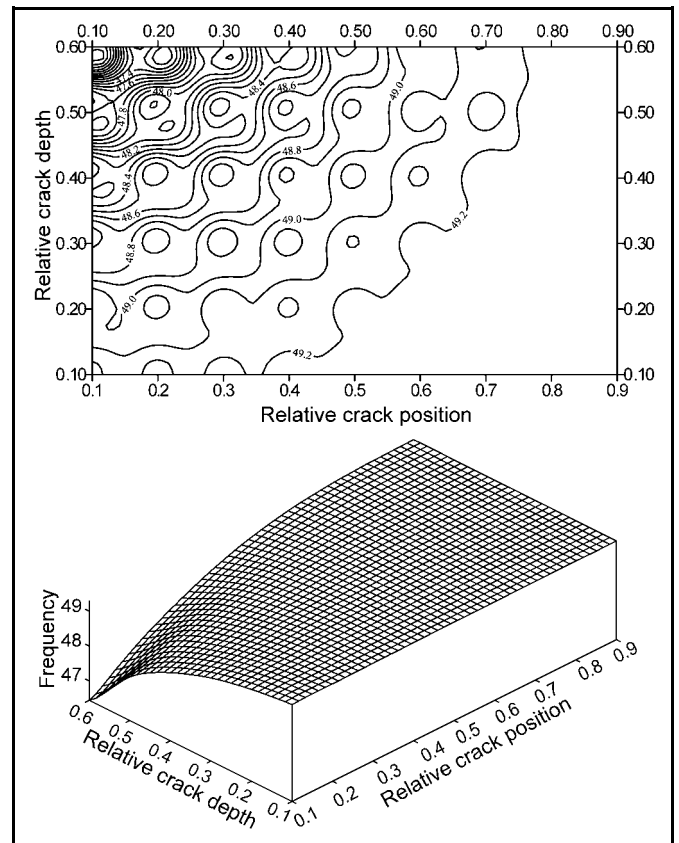
Figure 32. First fundamental frequencies of a cracked mild steel beam for various crack positions and depths. (a) Contours; (b) 3-D plot.
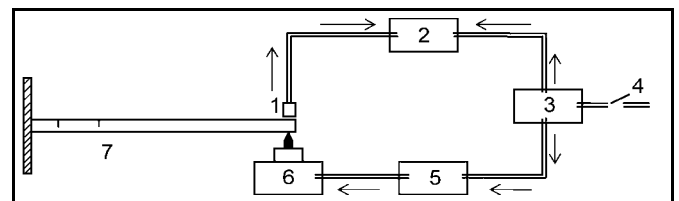
Figure 33. Schematic block diagram of experimental set-up. 1 - vibration pickup, 2 - vibration indicator, 3 - distribution box, 4 - power supply, 5 - power amplifier, 6 - vibration generator, 7 - cantilever beam specimen.

Table 1. Experimental results for aluminium beam ($L = 80$ cm, $B = 5$ cm, $W = 0.6$ cm).

Crack location L_1 (cm)	Crack location L_2 (cm)	Crack depth a_1 (cm)	Crack depth a_2 (cm)	Frequency (Hz)		
				first mode	second mode	third mode
5.0	10.0	0.1	0.1	48.0	302.3	846.0
5.0	10.0	0.2	0.1	47.6	301.7	845.9
5.0	10.0	0.2	0.2	47.4	301.6	842.5
5.0	10.0	0.3	0.3	46.0	300.0	834.5
5.0	10.0	0.4	0.4	42.2	295.0	812.0
10.0	20.0	0.1	0.1	48.0	302.3	845.9
10.0	20.0	0.1	0.2	47.8	302.2	842.5
10.0	20.0	0.2	0.1	47.6	301.7	842.5
10.0	20.0	0.2	0.2	47.4	301.6	842.5
10.0	20.0	0.3	0.1	46.7	300.0	842.5
10.0	20.0	0.3	0.2	46.5	300.0	842.4
10.0	20.0	0.3	0.3	46.0	300.0	834.6
10.0	20.0	0.4	0.2	44.0	296.8	835.2
10.0	20.0	0.4	0.3	43.6	296.5	834.0

The changes of dimensionless frequencies for the eigen values as a function of crack depth are shown in Figs. 27-30. It can be seen that measurable changes in natural frequencies can be observed for relatively deep cracks. 3-D and contour plots are drawn (Figs. 31 and 32) which show the variation of crack depth and crack position with respect to the natural frequency.

Aluminium beams ($900 \times 36 \times 6$ mm) with desired transverse cracks were used for determining natural frequencies and mode shapes. The experimental results for relative amplitude at different relative distances for the aluminium beam specimen having relative crack depths 0.334 and 0.334 and relative crack positions 0.125 and 0.5 are plotted in Figs. 34-36 for the first three modes. The corresponding numerical results are also presented for comparison.

Similarly, for the mild steel beam specimen ($900 \times 40 \times 6$ mm), for a similar crack geometry, the mode shapes from numerical and experimental analysis are plotted and compared (Figs. 37-39). The graph shows good agreement between the numerical and experimental results.

The current results were compared with the numerical results obtained by Fernandez et al.[20] (Fig. 40). It is observed that the current results agree well with the numerical ones. The numerical results for the frequency ratio with respect to relative crack position and depth are shown in Tables 2 and 3 for aluminium and mild steel beams respectively. From the given numerical results (Tables 2 and 3), the relative crack location or depth can be found out from the frequency ratio, and vice versa.

7. CONCLUSION

An analytical-computational method has been used for solving the frequency equation of an elastic cantilever beam with a single/multiple cracks. The position of the crack can be predicted from the deviations of the fundamental modes between the cracked and uncracked beams. Furthermore, the crack sizes can be identified by the variation of the corresponding natural frequencies. Thus, it is possible to monitor the growth of a crack in a beam, with the initially uncracked beam considered as the baseline for future measurement.

One can also construct a contour or 3-D plot of natural frequencies for each crack position and depth, as shown in Figs. 31 and 32. From these diagrams, the depth of the cracks can be determined from their cracked natural frequencies, if the position of the crack is known from the sharply changed curves of deviation of fundamental mode shapes.

The conclusions of the present study can be summarised as follows:

1) The presence of a crack in structural members introduces local flexibility, which can be computed and used in structural analysis.

2) The identification method is based on the assumption of transverse surface cracks extending uniformly along the width of structure.

3) This method is applicable to structural systems which have analytical description or can be modelled by means of FEM or some other convenient discretisation method. Furthermore, any complex structure can be broken into simple local structural members for vibration analysis by making proper assumptions. Suitable boundary conditions can be imposed on the local structural elements for vibration analysis.

Table 2. Variation of frequency ratio with respect to relative crack position and depth. Cracked aluminium beam ($L = 80$ cm, $B = 5$ cm, $W = 0.6$ cm).

| Relative crack position	Relative crack depth	Frequency ratio	Relative crack position	Relative crack depth	Frequency ratio
0.0625	0.02	0.979439	0.5	0.3	0.979439
0.0625	0.05	0.979437	0.5	0.4	0.97944
0.0625	0.1	0.979795	0.5	0.5	0.975375
0.0625	0.15	0.978184	0.5	0.6	0.971313
0.0625	0.2	0.975339	0.5	0.7	0.96212
0.0625	0.25	0.973343	0.5	0.8	0.936927
0.0625	0.3	0.971311	0.5	0.9	0.825396
0.0625	0.35	0.967247	0.6	0.01	0.981472
0.0625	0.4	0.961153	0.6	0.1	0.97944
0.0625	0.5	0.944895	0.6	0.2	0.97944
0.0625	0.6	0.918478	0.6	0.3	0.97944
0.0625	0.7	0.865826	0.6	0.4	0.97944
0.0625	0.8	0.753469	0.6	0.5	0.979439
0.0625	0.9	0.495418	0.6	0.6	0.975375
0.1	0.01	0.981469	0.6	0.7	0.972101
0.1	0.1	0.979439	0.6	0.8	0.960088
0.1	0.2	0.977407	0.6	0.9	0.899142
0.1	0.3	0.971311	0.7	0.01	0.97944
0.1	0.4	0.963183	0.7	0.1	0.97944
0.1	0.5	0.948959	0.7	0.2	0.97944
0.1	0.6	0.924574	0.7	0.3	0.97944
0.1	0.7	0.876585	0.7	0.4	0.97944
0.1	0.8	0.771551	0.7	0.5	0.979439
0.1	0.9	0.517974	0.7	0.6	0.979439
0.2	0.01	0.981471	0.7	0.7	0.97779
0.2	0.1	0.979439	0.7	0.8	0.973286
0.2	0.2	0.977407	0.7	0.9	0.94993
0.2	0.3	0.975359	0.8	0.01	0.97944
0.2	0.4	0.967247	0.8	0.1	0.97944
0.2	0.5	0.957087	0.8	0.2	0.97944
0.2	0.6	0.938798	0.8	0.3	0.97944
0.2	0.7	0.90381	0.8	0.4	0.97944
0.2	0.8	0.81889	0.8	0.5	0.97944
0.2	0.9	0.584017	0.8	0.6	0.979439
0.3	0.01	0.979439	0.8	0.7	0.980202
0.3	0.1	0.979439	0.8	0.8	0.979186
0.3	0.2	0.977407	0.8	0.9	0.974107
0.3	0.3	0.975176	0.9	0.01	0.97944
0.3	0.4	0.971312	0.9	0.1	0.97944
0.3	0.5	0.965215	0.9	0.2	0.97944
0.3	0.6	0.953023	0.9	0.3	0.97944
0.3	0.7	0.927585	0.9	0.4	0.97944
0.3	0.8	0.863993	0.9	0.5	0.979437
0.3	0.9	0.659203	0.9	0.6	0.97944
0.4	0.01	0.981471	0.9	0.7	0.981191
0.4	0.1	0.981471	0.9	0.8	0.980811
0.4	0.2	0.979439	0.9	0.9	0.980405
0.4	0.3	0.977408	0.99	0.01	0.97944
0.4	0.4	0.975376	0.99	0.1	0.97944
0.4	0.5	0.971311	0.99	0.2	0.97944
0.4	0.6	0.963184	0.99	0.3	0.97944
0.4	0.7	0.947315	0.99	0.4	0.97944
0.4	0.8	0.904216	0.99	0.5	0.97944
0.4	0.9	0.74169	0.99	0.6	0.979437
0.5	0.01	0.981472	0.99	0.7	0.980811
0.5	0.1	0.981471	0.99	0.8	0.980819
0.5	0.2	0.979439	0.99	0.9	0.980838
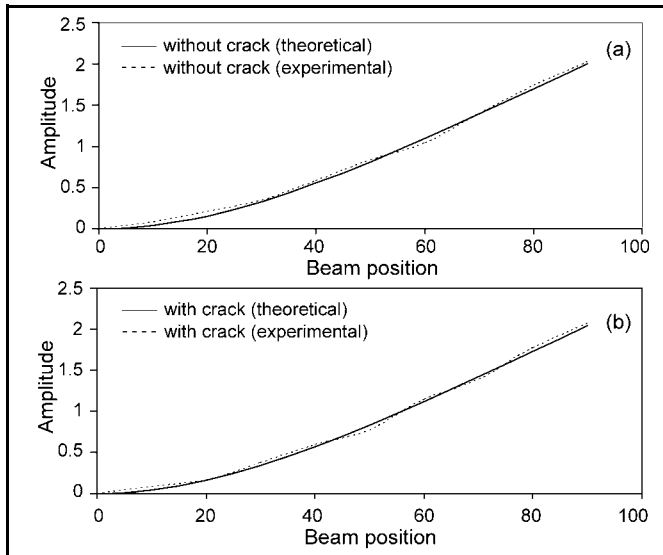
Figure 34. First mode of transverse vibration, aluminium beam ($\xi_1 = 0.334$, $\xi_2 = 0.334$, $\beta_1 = 0.125$, $\beta_2 = 0.25$).
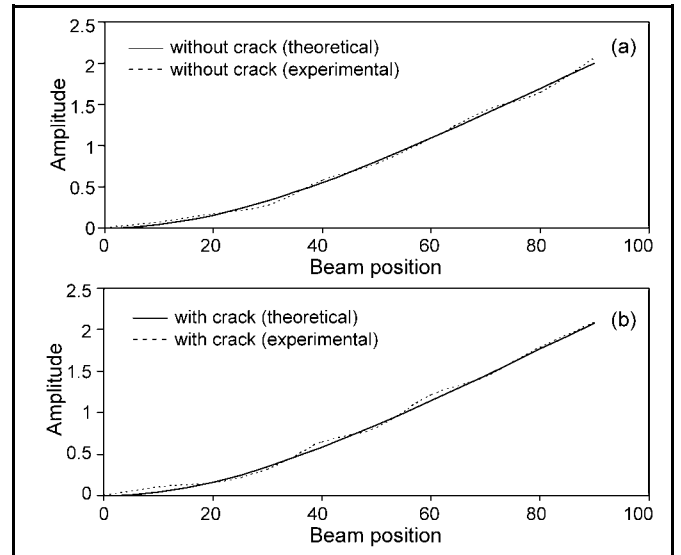

Figure 37. First mode of transverse vibration, mild steel beam ($\xi_1 = 0.334$, $\xi_2 = 0.334$, $\beta_1 = 0.125$, $\beta_2 = 0.25$).
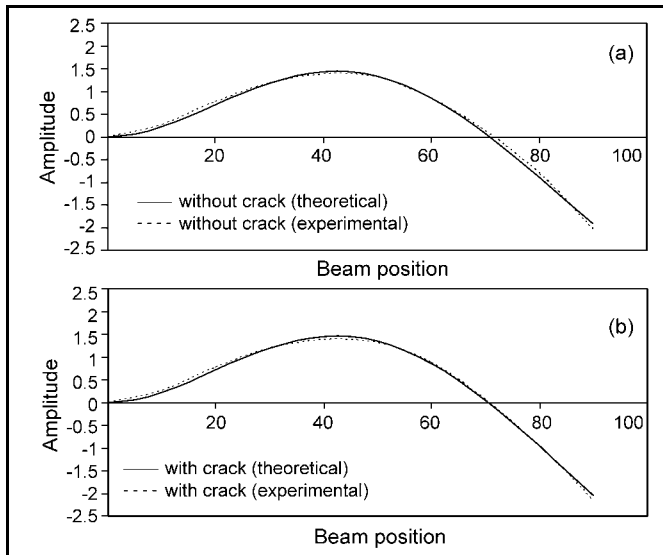

Figure 35. Second mode of transverse vibration, aluminium beam ($\xi_1 = 0.334$, $\xi_2 = 0.334$, $\beta_1 = 0.125$, $\beta_2 = 0.25$).
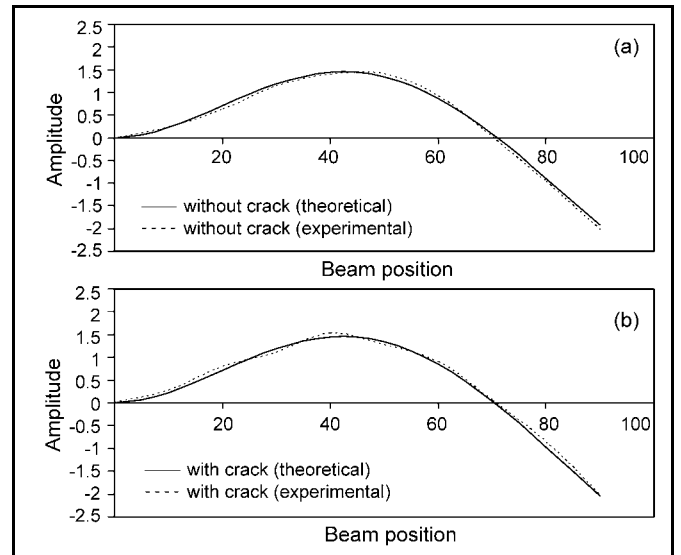

Figure 38. Second mode of transverse vibration, mild steel beam ($\xi_1 = 0.334$, $\xi_2 = 0.334$, $\beta_1 = 0.125$, $\beta_2 = 0.25$).
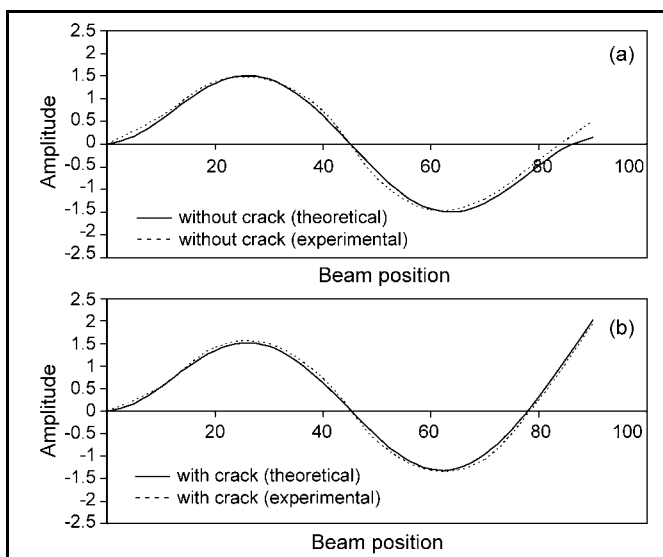

Figure 36. Third mode of transverse vibration, aluminium beam ($\xi_1 = 0.334$, $\xi_2 = 0.334$, $\beta_1 = 0.125$, $\beta_2 = 0.25$).
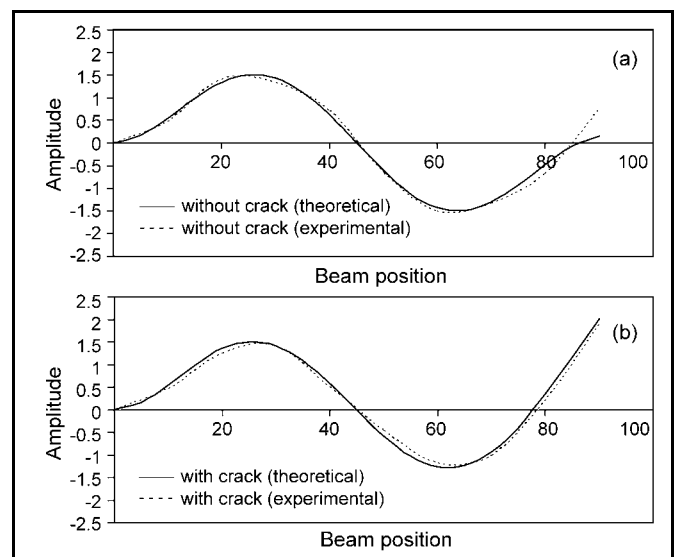

Figure 39. Third mode of transverse vibration, mild steel beam ($\xi_1 = 0.334$, $\xi_2 = 0.334$, $\beta_1 = 0.125$, $\beta_2 = 0.25$).
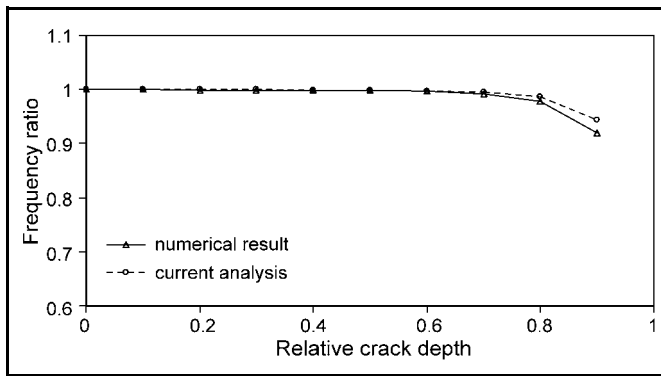
Figure 40. Comparison of numerical result (Fernandez et al.) with current analysis for variation of fundamental frequency with crack ratio of a cantilever beam, $L_1/L = 0.75$, $\omega_{uncrack} = 1280.796923$.

Table 3. Variation of frequency ratio with respect to relative crack position and depth. Cracked mild steel beam ($L = 80$ cm, $B = 5$ cm, $W = 0.6$ cm).

Relative crack position	Relative crack depth	Frequency ratio	Relative crack position	Relative crack depth	Frequency ratio
0.1	0.1	0.996114	0.5	0.4	0.994496
0.1	0.2	0.993282	0.5	0.5	0.992068
0.1	0.3	0.988197	0.5	0.6	0.987818
0.1	0.4	0.979522	0.6	0.1	0.997143
0.1	0.5	0.965357	0.6	0.2	0.997109
0.1	0.6	0.940063	0.6	0.3	0.996722
0.2	0.1	0.996536	0.6	0.4	0.996114
0.2	0.2	0.994496	0.6	0.5	0.9949
0.2	0.3	0.990853	0.6	0.6	0.992877
0.2	0.4	0.984783	0.7	0.1	0.997329
0.2	0.5	0.974463	0.7	0.2	0.997328
0.2	0.6	0.955846	0.7	0.3	0.997126
0.3	0.1	0.855068	0.7	0.4	0.996924
0.3	0.2	0.995525	0.7	0.5	0.996519
0.3	0.3	0.993079	0.7	0.6	0.99571
0.3	0.4	0.98883	0.8	0.1	0.997329
0.3	0.5	0.98195	0.8	0.2	0.997329
0.3	0.6	0.969202	0.8	0.3	0.997329
0.4	0.1	0.996944	0.8	0.4	0.997329
0.4	0.2	0.996114	0.8	0.5	0.997126
0.4	0.3	0.994698	0.8	0.6	0.996924
0.4	0.4	0.992068	0.9	0.1	0.997329
0.4	0.5	0.987818	0.9	0.2	0.997329
0.4	0.6	0.979926	0.9	0.3	0.997329
0.5	0.1	0.997143	0.9	0.4	0.997329
0.5	0.2	0.996695	0.9	0.5	0.997322
0.5	0.3	0.995912	0.9	0.6	0.997329

4) However, a database can be prepared for the different geometry of beams with cracks. The experimental results of beam-like structures used in a practical application can be compared with the results of the database. Hence, the location and size of a crack can be determined.

5) The analytical-computational method described in the paper provides accuracy for minute cracks.

6) The results obtained from the experimental analysis show excellent agreement with the corresponding numerical results.

The proposed method can be used as a technique and as a tool for preventive maintenance and the non-destructive test-ing of structures. The results from the current analysis can be utilised for the fault diagnosis of structures and for condition monitoring.

REFERENCES

[1] Papadopoulos, C. A. and Dimarogonas, A. D. Stability of cracked rotors in the coupled vibration mode, *Transactions of the ASME, Journal of Vibration, Acoustics, Stress, and Reliability in Design*, **110**, 356-359, (1988).

[2] Anifantis, N. and Dimarogonas, A. D. Stability of columns with a single crack subjected to follower and vertical loads, *International Journal of Solids and Structures*, **19** (3), 281-291, (1983).

[3] Gounaris, G. and Dimarogonas, A. D. A finite element of a cracked prismatic beam for structural analysis, *Computer and Structure*, **28** (3), 309-313, (1988).

[4] Chen, L.-W. and Chen, C.-Lu. Vibration and stability of cracked thick rotating blades, *Computer and Structure*, **28** (1), 67-74, (1988).

[5] Dimarogonas, A. D. and Papadopoulos, C. A. Vibration of cracked shaft in bending, *Journal of Sound and Vibration*, **91** (4), 583-593, (1983).

[6] Cawley, P. and Adams, R. D. The location of defects in structures from measurements of natural frequencies, *Journal of Strain Analysis*, **14** (2), 49-57, (1979).

[7] Papadopoulos, C. A. and Dimarogonas, A. D. Coupled vibration of cracked shafts, *Transactions of the ASME, Journal of Vibration and Acoustics*, **114** (3), 461-467, (1992).

[8] Gudmundson, P. The dynamic behaviour of slender structures with cross sectional cracks, *Journal of Mechanics and Physics of Solids*, **31** (4), 329-345, (1983).

[9] Chondros and Dimarogonas, A. D. Identification of cracks in circular plates welded at the contour, *ASME Design Engineering Technical Conference*, St. Louis, USA, September, Paper No.79-DET-106, (1979).

[10] Gounaris, G. and Papazoglou, V. Three-dimensional effects on the natural vibrations of cracked Timoshenko beams in water, *Computer and Structure*, **42** (5), 769-779, (1992).

[11] Papadopoulos, C. A. and Dimarogonas, A. D. Coupled longitudinal and bending vibration of a rotating shaft with an open crack, *Journal of Sound and Vibration*, **117** (1), 81-93, (1987).

[12] Papadopoulos, C. A. and Dimarogonas, A. D. Coupled longitudinal and bending vibrations of a cracked shaft, *Journal of Vibration, Acoustics, Stress, and Reliability in Design*, **110**, 1-8, (1988).

[13] Dimarogonas, A. D. and Massouros, G. Torsional vibration of a shaft with a circumferential crack, *Engineering Fracture mechanics*, **15** (3-4), 439-444, (1981).

[14] Tsai, T. C. and Wang, Y. Z. Vibration analysis and diagnosis of a cracked shaft, *Journal of Sound and Vibration*, **192** (3), 607-620, (1996).

[15] Anifantis, N. and Dimarogonas, A. D. Imperfection post-buckling analysis of cracked columns, *Engineering Fracture Mechanics*, **18** (3), 693-702, (1983).

[16] Dado, M. H. Comprehensive crack identification algorithm for beams under different end conditions, *Applied Acoustics*, **51** (4), 381-398, (1997).

[17] Chinchalkar, S. Determination of crack location in beams using natural frequencies, *Journal of Sound and Vibration*, **247** (3), 417-429, (2001).

[18] Saavedra, P. N. and Cuitino, L. A. Crack detection and vibration behaviour of cracked beams, *Computers and Structures*, **79** (16), 1451-1459, (2001).

[19] Sinha, J. K. and Friswell, M. I. Simulation of the dynamic response of a cracked beam, *Computers and Structures*, **80** (18-19), 1473-1476, (2002).

[20] Fernandez-Saez, J. and Navaro, C. Fundamental frequency of cracked beam in bending vibrations: an analytical approach, *Journal of Sound and Vibration*, **256** (1), 17-31, (2002).

[21] Stephen H. C., Norman, C. D., and Thomas, J. L. *An Introduction to the Mechanics of Solids*, McGraw-Hill Book Company, Second Edition, (1978).

[22] Tada, H., Paris, P. C., and Irwin, G. R. *The Stress Analysis of Cracks Handbook*, Third Edition, ASME PRESS, (2000).

[23] Dimarogonas, A. D. and Haddad, S. *Vibration for Engineers*, Prentice Hall, Englewood Cliffs, New Jersey 07632, (1992).